Mon. Not. R. Astron. Soc. **000**, 000–000 (0000) Printed 3 September 2015 (MN LATEX style file v2.2)

The Alignment of the Velocity Ellipsoid in Galaxies

N. W. Evans[1], J. L. Sanders[1], A. A. Williams[1], J. An[2], D. Lynden-Bell[1], and W.Dehnen[3]

[1]*Institute of Astronomy, University of Cambridge, Madingley Road, Cambridge, CB3 0HA, UK*
[2]*National Astronomical Observatories, Chinese Academy of Sciences, A20 Datun Road, Chaoyang District, Beijing 100012, PR China*
[3]*Department for Physics & Astronomy, University of Leicester, Leicester, LE1 7RH, United Kingdom*

3 September 2015

ABSTRACT

We study the alignment of the velocity ellipsoid in stellar systems. We prove that if the velocity ellipsoid is everywhere exactly aligned in spherical polar coordinates, then the gravitational potential must be of separable or Stäckel form (excepting degenerate cases where two or more of the semiaxes of the velocity ellipsoid are everywhere the same). This is under the assumption that the DF is reflection-symmetric in velocity space. More generally, we show that provided the principal axes are generally unequal and are oriented perpendicular to a set of orthogonal surfaces at each point, then those surfaces must be confocal quadratic surfaces. Furthermore, the gravitational potential must be separable in the corresponding coordinate system and the three independent integrals are quadratic in the velocities. Thus we provide a new, more powerful, proof of Eddington's theorem which does not rest on the restrictive ellipsoidal hypothesis. In particular, the theorem holds true for alignment in cylindrical polar coordinates, which is used in the popular Jeans Anisotropic Models (JAM) of Cappellari (2006). It follows that the only physical JAM solutions correspond to unrealistic separable potentials in cylindrical polars.

We analyse data on the radial velocities and proper motions of a sample of ~ 7300 stars in the stellar halo of the Milky Way. The stars lie between $6 < R < 11$ kpc and $3 < |z| < 5$ kpc, where R and z are Galactocentric cylindrical polar radius and height. We demonstrate that the velocity distributions are reflection-symmetric. By Monte Carlo simulations, we provide the distributions of the tilt angles or misalignments from both the spherical polar and prolate spheroidal coordinate systems. We show that in this sample the misalignment is always small ($\lesssim 7$ degrees) in the Northern hemisphere, though there are some deviations in the Southern hemisphere. Alignment in a prolate spheroidal coordinates with focal distance distance $a = 5.21 \pm 0.66$ kpc gives a marginally better fit than spherical alignment.

We proceed to construct a realistic model of a triaxial stellar halo in a triaxial NFW dark matter halo using a made-to-measure method. Our model is chosen to have a anisotropy profile that goes from isotropic to highly radial in the outskirts. We find that, despite the triaxiality of the potential, the velocity ellipsoid of the stellar halo is nearly spherically aligned within ~ 6 degrees for large regions of space, particularly outside the scale radius of the stellar halo. We thus conclude that the velocity ellipsoid can be close to spherically aligned for a much wider class of potentials than the strong constraints that arise from exact alignment might suggest.

Key words: galaxies: haloes – galaxies: kinematics and dynamics – stellar dynamics – dark matter

1 INTRODUCTION

The Jeans equations relate the gravitational potential of a galaxy to the components of the velocity dispersion tensor. This is an attractive way to infer properties of the mass distribution, without the complexities of specifying a full phase space distribution function (DF).

The components of the velocity dispersion tensor of a stellar population are defined as

$$\sigma_{ij}^2 \equiv \Big\langle (v_i - \langle v_i \rangle)(v_j - \langle v_j \rangle) \Big\rangle , \qquad (1)$$

where the subscript indices denote one of the orthogonal coordinate directions, and the angled brackets represent averaging over the phase space distribution function (see e.g., Binney & Tremaine 2008). The dispersion tensor is a symmetric second-rank tensor and so may always be diagonalized. The principal axes of the tensor then form a velocity ellipsoid. This paper studies the alignment of

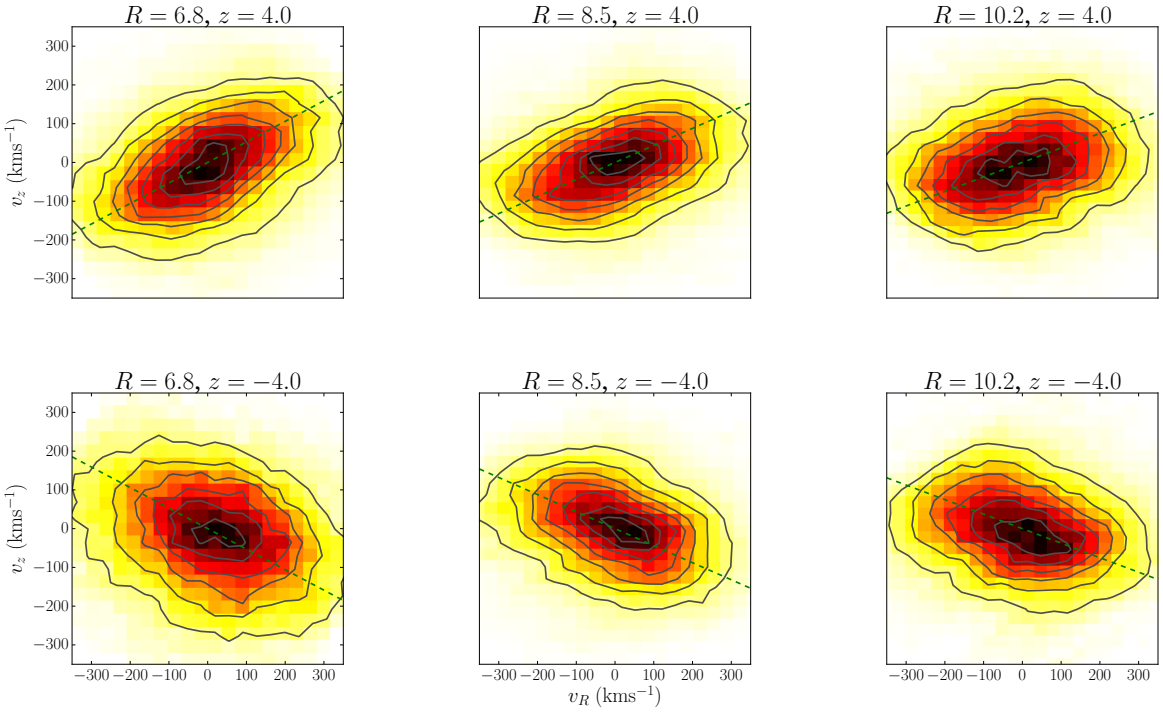

Figure 1. Velocity distributions of our halo sample in (v_R, v_z) space in 6 spatial bins. The position of each bin centroid (R, z) is written in kpc above the plot of the velocity distributions in that bin. The green dashed lines are at an angle $\arctan(z/R)$ where (R, z) is the position of the bin centroid. The long axis of the (v_R, v_z) distribution should coincide with this line if the velocity ellipsoid is spherically aligned.

the velocity ellipsoid and its implications for the underlying gravitational potential.

The Jeans equaions are the first-order moments of the collisionless Boltzmann equation. They are three equations relating the six independent components of the dispersion tensor σ_{ij}^2 to the density and the potential. Hence, the Jeans equations cannot uniquely determine the σ_{ij}^2 and some closure condition must be adopted. A common choice is the alignment of the velocity ellipsoid im some coordinate system, which reduces the number of independent variables from six to three – namely, the semiaxes of the velocity ellipsoid. For example, Cappellari (2008) provided an elegant way to solve the Jeans equations, assuming alignment in the cylindrical polar coordinate system (R, ϕ, z). These models – Jeans anisotropic models or JAM – have become widely used in analyses of integral field data on elliptical galaxies (see e.g., McDermid et al. 2015), as well as studies of nuclear clusters (Hartmann et al. 2011) and lensing galaxies (van de Ven et al. 2010). Cylindrically aligned solutions with two of the semiaxes equal (i.e., $\langle v_R^2 \rangle = \langle v_z^2 \rangle$) are generated by distribution functions depending on the two isolating integrals, energy E and angular momentum component L_z (Jeans 1919). When all three semiaxes are different, the validity of the JAM solutions remains unclear. In fact, Binney (2014) has already questioned whether construction of numerical DFs for models with such properties is possible.

Alignment in the spherical polar coordinate system (r, θ, ϕ) is also often used in the Jeans equations. If two of the semiaxes are equal (i.e., $\langle v_\theta^2 \rangle = \langle v_\phi^2 \rangle$), then the spherical aligned solutions can be generated by distribution functions depending on the two integrals, energy E and square of the angular momentum L^2. Assuming a spherical density and potential, this ansatz is very popular as the Jeans equations then reduce to a single equation for the radial velocity dispersion $\langle v_r^2 \rangle$ together with an anisotropy parameter $\beta(r)$

$$\beta(r) = 1 - \frac{\langle v_\theta^2 \rangle}{\langle v_r^2 \rangle}. \qquad (2)$$

Given a choice for $\beta(r)$, the only non-trivial Jeans equations can be straightforwardly solved using an integrating factor (see e.g., van der Marel 1994; An & Evans 2011; Agnello et al. 2014). Algorithms for solution of the Jeans equations using spherical alignment but flattened densities and potentials have also been developed (see e.g., Bacon et al. 1983; Bacon 1985; Evans et al. 1997, 2015). These can in general have three different principal axes $\langle v_r^2 \rangle$, $\langle v_\theta^2 \rangle$ and $\langle v_\phi^2 \rangle$ and so the velocity ellipsoid is triaxial, but whether they can be realised by physical (non-negative) distribution functions remains unclear.

Alignment in spheroidal coordinates (λ, μ, ϕ) has also been studied. This coordinate system is described in, for example, Morse & Feshbach (1953) or Binney & Tremaine (2008). Within the foci of the coordinate system, spheroidal alignment approaches cylindrical, whilst at large radii, it tends to spherical. Spheroidal alignment can therefore be viewed as interpolating between these two more familiar cases. It has long been known that if the gravitational potential is of Stäckel or separable form, then the velocity ellipsoid is aligned in spheroidal coordinates (see e.g., Eddington 1915; Lynden-Bell 1962; Evans & Lynden-Bell 1989). However, the assumption that the velocity ellipsoid is aligned in spheroidal coordinates can be made without a separable potential (Arnold 1995). In fact, this makes good sense, as models of axisymmetric galaxies

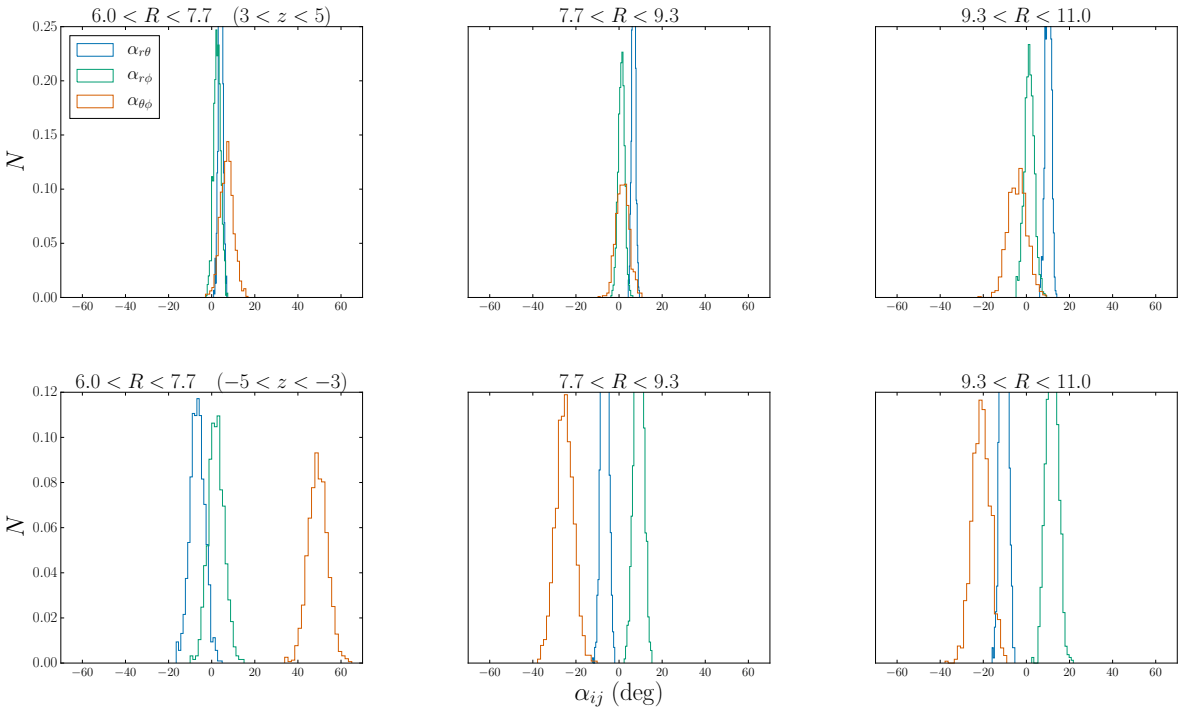

Figure 2. The distribution of spherical tilt angles $\alpha_{r\theta}$ (blue), $\alpha_{r\phi}$ (green) and $\alpha_{\theta\phi}$ (red) in degrees at 6 equally spaced locations in Galactocentric cylindrical polars (R, z) with $6 \le R \le 11$ kpc and $3 \le |z| \le 5$ kpc. Written above each plot is the position of the centroid of the bin in question. A summary of these distributions can be found in Table 1.

(R,z) (kpc)	$\alpha_{r\theta}$ (deg)	$\Delta\alpha_{r\theta}$ (deg)	$\alpha_{r\phi}$ (deg)	$\Delta\alpha_{r\phi}$ (deg)	$\alpha_{\theta\phi}$ (deg)	$\Delta\alpha_{\theta\phi}$ (deg)
(6.85,4.00)	4.22	0.99	2.50	1.80	7.18	3.12
(8.50,4.00)	6.80	0.85	1.03	1.47	1.86	2.88
(10.15,4.00)	10.22	1.27	1.21	2.34	-4.18	4.37
(6.85,-4.00)	-6.58	3.57	2.00	3.69	48.80	4.50
(8.50,-4.00)	-6.60	1.58	9.20	2.06	-24.75	4.08
(10.15,-4.00)	-10.42	1.64	12.05	2.66	-20.75	4.22

Table 1. At each location (R, z), the means and dispersions in the three spherical tilt angles are given.

using numerical constructed DFs do suggest the alignment may be close to spheroidal (e.g., Dehnen & Gerhard 1993; Binney 2014). Intuitively, for systems like the stellar halo of the Milky Way, the potential in the inner parts is controlled by the flattened disk and bulge, in the outer parts by the rounder dark matter halo, and so again an alignment in spheroidal coordinates does seems very natural.

Spheroidal coordinates are the axisymmetric limit of ellipsoidal coordinates (λ, μ, ν). For triaxial Stäckel models, Eddington (1915) already knew that the velocity ellipsoid is aligned in ellipsoidal coordinates. The triaxial Jeans equations for such Stäckel systems have been studied sporadically (Lynden-Bell 1960; Evans & Lynden-Bell 1989; van de Ven et al. 2003). Given the density and potential, the Jeans equations are now three coupled first-order partial differential equations for three unknowns, namely $\langle v_\lambda^2\rangle$, $\langle v_\nu^2\rangle$ and $\langle v_\mu^2\rangle$. Both the prescription of appropriate boundary conditions and the solution of the equations is challenging. Only very few general triaxial DFs have ever been numerically constructed. The few such models available do show approximate alignment in ellipsoidal coordinates (e.g., Sanders & Evans 2015).

Our intention in this paper is to examine what may be legitimately deduced about the underlying gravitational potential from the alignment of the velocity ellipsoid. This is motivated by arguments of Smith et al. (2009a) who claim that: "If a steady state stellar population has a triaxial velocity dispersion tensor whose eigenvectors are everywhere aligned in spherical polar coordinates, then the underlying gravitational potential must be spherically symmetric". This theorem will be examined, slightly corrected, and then extended below.

This argument was queried by Binney & McMillan (2011), who created a torus-based model of the Galaxy that, at locations above the plane of the Milky Way, possessed a spherically aligned velocity dispersion tensor, even though the potential was highly flattened. Although Binney & McMillan (2011) did not provide an explicit counter-example to the theorem of Smith et al. (2009a), they did question whether in general the potential does control the tilt. In their numerically constructed example, they argued that the tilt of the velocity ellipsoid is controlled at least as much by the weightings of orbits, and hence the DF, as compared to the potential. In this respect, Binney & McMillan (2011) conjectured that insights from separable or Stäckel models may not tell the whole story. One of the aims of this paper is to resolve the tension between these two viewpoints.

The paper is organised as follows. Section 2 studies the one

(R, z)	β	$\Delta\beta$
(6.85,4.00)	0.538	0.014
(8.50,4.00)	0.565	0.012
(10.15,4.00)	0.485	0.017
(6.85,-4.00)	0.487	0.039
(8.50,-4.00)	0.516	0.020
(10.15,-4.00)	0.452	0.021

Table 2. At each location (R, z), the means and dispersions in the spherical anisotropy parameter β are given.

(R, z) (kpc)	$\alpha_{\lambda\mu}$ (deg)	$\Delta\alpha_{\lambda\mu}$ (deg)	$\alpha_{\lambda\phi}$ (deg)	$\Delta\alpha_{\lambda\phi}$ (deg)	$\alpha_{\mu\phi}$ (deg)	$\Delta\alpha_{\mu\phi}$ (deg)
(6.85,4.00)	-3.77	1.00	1.96	1.72	8.03	2.91
(8.50,4.00)	1.51	0.85	0.96	1.46	2.04	2.76
(10.15,4.00)	6.47	1.27	1.31	2.32	-3.76	3.84
(6.85,-4.00)	1.25	3.44	-0.39	3.70	49.62	4.21
(8.50,-4.00)	-1.43	1.52	8.28	2.15	-25.35	3.79
(10.15,-4.00)	-6.80	1.61	10.92	2.80	-20.91	3.84

Table 3. At each location (R, z), the means and dispersions in the three spheroidal tilt angles (using $a = 5.21$ kpc, our maximum–likelihood focal distance) are given.

spheroidal system for which there is hard data on the alignment – namely, the stellar halo of the Milky Way galaxy. For elliptical galaxies, evidence on the alignment is necessarily much more indirect, as only the line of sight velocity distribution can be measured. We confirm, and sharpen, the results of Smith et al. (2009a) and Bond et al. (2010) that the velocity ellipsoid of stars in the Milky Way stellar halo is close to spherical or spheroidal alignment. Section 3 is theoretical and examines the case of exact spherical alignment. We prove under quite general conditions that the gravitational potential must be of separable or Stäckel form in spherical polars. This is an elaboration of the original theorem of Smith et al. (2009a). The only exceptions are simpler cases in which the velocity ellipsoid has either two axes the same and so is a spheroid, or three axes the same and so is a sphere. Section 4 discusses cylindrical and spheroidal alignment, and demonstrates, for the first time, that the assumption of alignment of the (assumed triaxial) dispersion tensor implies separability of the Hamilton-Jacobi equation in these coordinates. The converse result – that the separable or Stäckel potentials generate galaxy models in which the velocity dispersion tensor is aligned along the separable coordinate system – has been known for some time and is implicit in Eddington's and Chandrasekhar's early work (Eddington 1915; Chandrasekhar 1942; Evans 2011). Lastly, Section 5 builds models of stellar haloes in which the velocity dispersion tensor is close to, but not exactly, spherically aligned and tests whether results remain valid in this approximate regime. We show that it is possible to build haloes in flattened potentials in which the velocity ellipsoid is close to spherical alignment over substantial portions of configuration space, though not everywhere. However, the more the potential is flattened, the greater is the magnitude and extent of the misalignment.

2 THE STELLAR HALO OF THE MILKY WAY

2.1 Background

The study of the kinematics of stars in the Milky Way halo has been revolutionized by high quality data derived from the Sloan Digital Sky Survey (SDSS). Line of sight velocities are extracted from SDSS spectroscopy. Proper motions are derived from either multi-epoch SDSS photometry in Stripe 82 (Bramich et al. 2008) or from matches to archival Schmidt photographic-plate based catalogues (Munn et al. 2004). So, all three components of velocities are now available for thousands of halo stars, together with positions and photometric parallaxes.

Smith et al. (2009a,b) constructed a sample of halo subdwarfs using a reduced proper motion diagram, utilizing the light-motion catalog for Stripe 82 (Bramich et al. 2008). They extracted a clean sample of 1,782 halo stars, lying at Galactocentric cylindrical polar radii between 7 and 10 kpc, and at depths of 4.5 kpc or less below the Galactic plane. They found that the velocity ellipsoid of the halo stars is aligned with the spherical polar coordinate system, with the long axis pointing towards the Galactic Centre. The halo stars are strongly radially anisotropic. The semiaxes of the velocity ellipsoid are $(\sigma_r, \sigma_\theta, \sigma_\phi) = (143 \pm 2, 77 \pm 2, 82 \pm 2)$ kms^{-1}, which corresponds to an anisotropy parameter

$$\beta = 1 - \frac{\sigma_\theta^2 + \sigma_\phi^2}{2\sigma_r^2} \tag{3}$$

of 0.69. They also noted a tentative asymmetry in the v_ϕ distribution, but found the v_r and v_θ distributions symmetric.

This conclusion was reinforced by the larger sample of Bond et al. (2010). Here, halo stars are extracted from the SDSS data by combined colour and metallicity cuts (specifically $0.2 < g-r < 0.4$ and [Fe/H] < -1.1). Requiring the stars possess SDSS spectra for radial velocities and POSS astrometry for proper motions yields a large sample of $\sim$ 7400 halo stars, with an estimated contamination of $\sim$ 6 per cent. Bond et al. (2010) found that the shape of the velocity ellipsoid is invariant in spherical coordinates within the volume probed by SDSS and aligned in spherical polar coordinates (their Figures 12 and 13). They found no statistically significant tilt from spherical alignment, with deviations modest and ranging between 1° to 5°. Note that this sample extends over Galactocentric cylindrical polar radii $6 \lesssim R \lesssim 11$ kpc and height above the Galactic plane $3 \lesssim z \lesssim 5$ kpc, and so is much more extensive than earlier work. Nonetheless, the semiaxes of the velocity ellipsoid are $(\sigma_r, \sigma_\theta, \sigma_\phi) = (141 \pm 5, 75 \pm 5, 85 \pm 5)$ kms^{-1}, in very good agreement with Smith et al. (2009b). Bond et al's error bars also include systematic effects such as errors in the photometric parallaxes, whereas Smith et al's do not.

Very recently, King et al. (2015) have examined a still larger sample of halo stars with Galactocentric radii between 6 and 30 kpc. This contains blue horizontal branch (BHB) and halo F stars extracted from SDSS, as well as a sample of still more distant F stars obtained from Hectospec on the MMT. Although only line of sight velocities are available, this still can yield constraints on the alignment, as there are different contributions from both radial and tangential velocities in different directions on the sky. King et al. (2015) find the alignment of the velocity ellipsoid of their halo sample to be close to spherical, albeit to within quite large uncertainties.

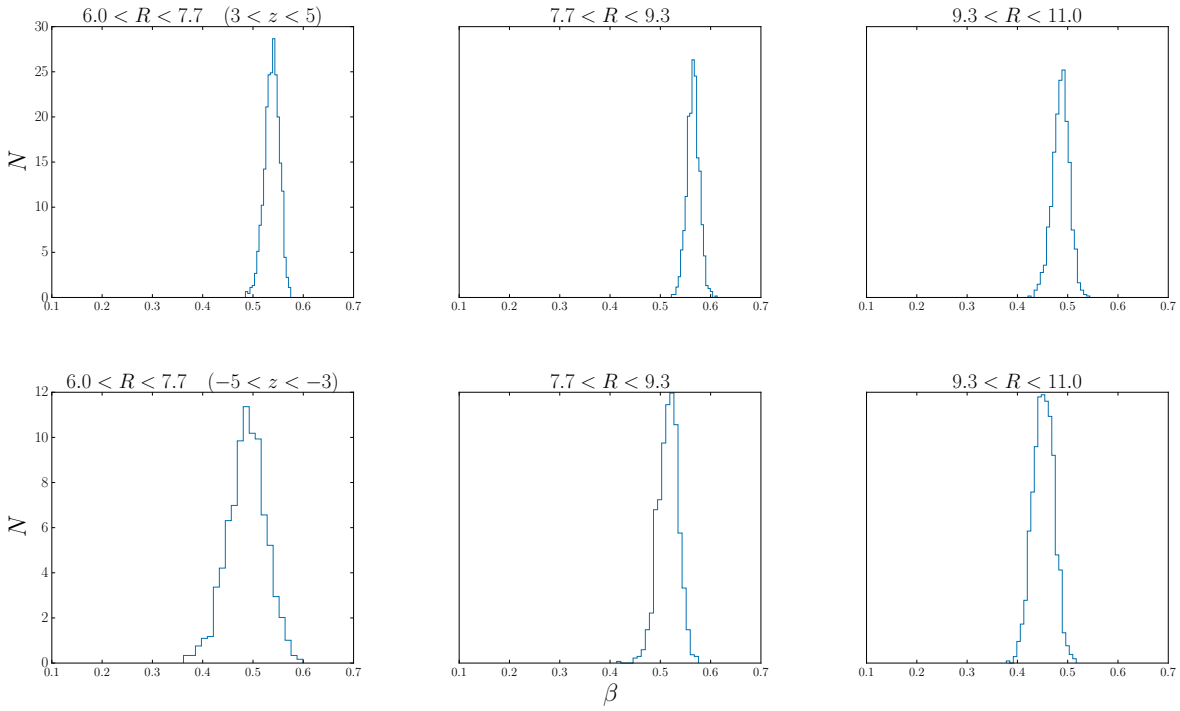

Figure 3. Probability distributions of the anisotropy parameter β obtained via Monte Carlo modelling in our spatial bins. The SDSS data imply a strongly radial velocity distribution, with $\beta \sim 0.5$ in all spatial bins.

(R, z) (kpc)	$p(r)$	$p(\theta)$	$p(\phi)$	$p(\lambda)$	$p(\mu)$
(6.85,4.00)	0.506	0.557	0.007	0.501	0.549
(8.50,4.00)	0.473	0.353	0.018	0.383	0.454
(10.15,4.00)	0.123	0.181	0.427	0.121	0.227
(6.85,-4.00)	0.440	0.457	0.538	0.434	0.379
(8.50,-4.00)	0.139	0.467	0.164	0.159	0.485
(10.15,-4.00)	0.424	0.525	0.505	0.464	0.508

Table 4. Median probabilities that the distribution of each velocity component is symmetric about zero. For each Monte–Carlo realisation of our sample and in each spatial bin, we perform a KS test on the two sides of each velocity distribution. After many resamples, we are left with distributions of the KS probability for each velocity component in each spatial bin. In general, these distributions are essentially flat between 0 and 1, which is consistent with a symmetric velocity distribution within the errors. In two cases, the v_ϕ distribution appears to have significant evidence for skew ($p \sim 0.01$), which could be a consequence of disk contamination, or rotation in the stellar halo population close to the disk. There are also several other bins where one or more of the velocities have median probabilities ~ 0.1, which may be due to substructure in the data. Spheroidal velocity components v_λ and v_μ are computed using our maximum–likelihood focal distance, $a = 5.21$ kpc.

2.2 Alignment and Symmetries

Here, we will re-analyse the data of Bond et al. (2010). We first discuss how the errors on the observable quantities propagate through to the alignment. The errors on the radial velocities are computed by the SDSS pipeline, to which should be added a systematic error of between 2 kms^{-1} (optimistic) and 6 kms^{-1} (pessimistic). The proper-motion errors are discussed in Bond et al. (2010), who suggest using a fixed value of 0.6 mas yr^{-1}. We assume that there is zero covariance between the two proper-motion components.

The SDSS pipeline provides photometric errors, which can be used to compute random errors in absolute magnitude (assuming that the inter-band covariances are negligible). Polynomial relations for the absolute magnitude of F and G stars as a function of g, r, i and metallicity [Fe/H] are given in Ivezić et al. (2008). We then use Monte Carlo methods to gain an estimate of the random error in the absolute magnitude, given the errors in g,r,i and [Fe/H], and add 0.1 mag in quadrature to account for systematics. Given the estimates of error in the absolute magnitude (with systematics included), we use Monte Carlo methods to estimate the error on the distances of each star in the sample.

To extract the halo sample, we apply the cuts $0.2 < g-r < 0.6$ and $-3.0 <$ [Fe/H] < -1.1 to the data. With the remaining 48105 stars, we create Monte Carlo samples in (R, z) and (v_r, v_θ, v_ϕ) by drawing from Gaussians in line-of-sight distance, proper motions and line-of-sight velocities using the above error estimates and then performing coordinate transforms to get the relevant quantities. Once this is done, we cut the Monte Carlo sample in distance using $6 < R < 11$ kpc and $3 < |z| < 5$ kpc, where R and z are Galactocentric cylindrical polar radius and height z. Finally, we remove stars with $|v_i| > 400$ kms^{-1} ($i = r, \theta, \phi$). This leaves us with Monte Carlo samples of size ~ 7300.

Figure 1 depicts the combined velocity distributions of 100 of our Monte-Carlo halo samples. Just through visual inspection, it is clear that the velocity ellipsoid cannot be aligned with cylindrical coordinates, as the (v_R, v_z) distribution has a noticeable tilt. The

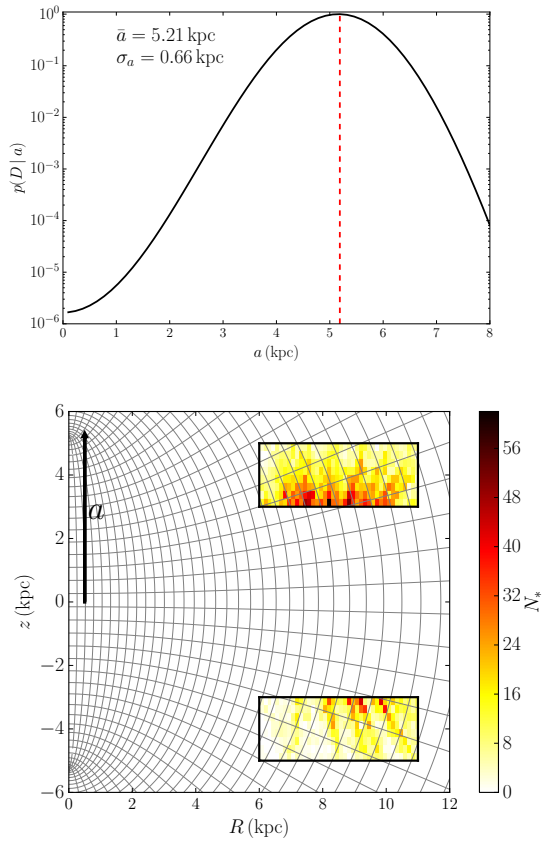

Figure 4. Top: the likelihood distribution $p(D\,|\,a)$ given 1000 Monte-Carlo samples of the data. We find $a = 5.21 \pm 0.66\,\mathrm{kpc}$. Bottom: lines of constant λ and μ in the best–fit spheroidal coordinate system. Overplotted is a histogram of a Monte–Carlo sample of the data within our spatial cuts.

green dashed lines in the plot are at an angle $\arctan(z/R)$, the direction that the long axis of the distribution should point if spherical alignment is satisfied. By eye, the tilt of the velocity distributions seems to be in good agreement with spherical alignment. This motivates a quantitative analysis of the data.

2.2.1 *Spherical alignment*

Given three orthogonal velocity components, (v_i, v_j, v_k), the tilt angle, α_{ij}, is the angle between the i-axis and the major axis of the ellipse formed by projecting the three dimensional velocity ellipsoid onto the ij-plane (see e.g., Binney & Merrifield (1998) or Appendix A of Smith et al. (2009a)).

$$\tan(2\alpha_{ij}) = \frac{2\sigma_{ij}^2}{\sigma_{ii}^2 - \sigma_{jj}^2}. \tag{4}$$

We compute the three independent tilt angles in 6 fixed, equal size, spatial bins in R and z. Figure 2 gives us probability distributions in the three misalignment angles in each bin. The $\alpha_{\theta\phi}$ distribution is the broadest, and this is understandable as the velocity second moments $\langle v_\theta^2 \rangle$ and $\langle v_\phi^2 \rangle$ are comparable (Smith et al. 2009b; Bond et al. 2010) and so the velocity ellipsoid is almost a spheroid. The distributions of $\alpha_{r\theta}$ and $\alpha_{r\phi}$ are narrower. The means and standard deviations of these histograms are listed in Table 1 for each of the 6 spatial bins. Figure 3 depicts the distributions of the anisotropy parameter in our spatial bins, which peak at $\beta \sim 0.5$ in all the bins, demonstrating that the stellar halo is a strongly radially biased population. The values of the anisotropy parameter for each bin are listed in Table 2. We have made no attempt to extract substructure from the data, so this can affect the measurements in some bins. Nonetheless, the overall picture is of a strongly radially anisotropic population ($\beta \sim 0.5$) that is close to spherical alignment above the plane. Below the plane, however, is a different story: significant evidence for misalignment is seen in these bins. There are several reasons as to why this might be. First, we possess fewer stars below the plane as compared to above it (see bottom panel of Figure 4). Our Gaussian model for the error distributions in the observables (as well as the error estimates themselves) may be oversimplified, and so the dispersions of the misalignment angle distributions may be underestimated. This could also be evidence for unrelaxed substructure in this part of the stellar halo. However, we shall see later that it is possible for variation in the misalignment angle such as is seen here to simply be a consequence of the DF and the potential.

2.2.2 *Spheroidal alignment*

Another coordinate system of interest is the prolate spheroidal system (λ, μ, ϕ). These coordinates (which are discussed in greater detail in Section 4.2) are related to cylindrical polars via the set of equations

$$\begin{aligned} R &= a\,\sinh\lambda\,\sin\mu, \\ z &= a\,\cosh\lambda\,\cos\mu, \\ \phi &= \phi. \end{aligned} \tag{5}$$

Surfaces of constant μ are hyperbolic sheets, whereas surfaces of constant λ are prolate ellipsoids. The quantity a is called the *focal distance*. At large distances from the origin, these surfaces begin to coincide with spherical polar coordinates ($\lambda \sim r$ and $\mu \sim \theta$), whereas at small distances the coordinate surfaces align with cylindrical polars ($\lambda \sim R$ and $\mu \sim z$). In order to compute properties of the velocity distributions, we must also express the velocities in this coordinate system. These are related to the cylindrical velocities via

$$\begin{aligned} v_\lambda &= \frac{v_R \cosh\lambda \sin\mu + v_z \sinh\lambda \cos\mu}{\sinh^2\lambda + \sin^2\mu}, \\ v_\mu &= \frac{v_R \sinh\lambda \cos\mu - v_z \cosh\lambda \sin\mu}{\sinh^2\lambda + \sin^2\mu}, \\ v_\phi &= v_\phi. \end{aligned} \tag{6}$$

Since there is a free parameter associated with this coordinate system, a, there are many possible different orientations of the velocity ellipsoids. In order to find the coordinate system in which the velocity distributions of our data are best aligned, we employed a maximum–likelihood technique. The likelihood is given by

$$p(D\,|\,a) = \prod_{\mathrm{bins}} \int_{\mathrm{errors}} d\boldsymbol{L}\, \exp\left[-\frac{1}{2} \sum_{\langle ij \rangle} \frac{\alpha_{ij}^2}{\sigma_{ij}^2} \right], \tag{7}$$

where α_{ij} is the misalignment angle given by Equation (4), D is the data, $\boldsymbol{L}$ are the observed quantities and the sum in the exponent is over all pairs of velocities. We approximate this likelihood using the principle of Monte–Carlo integration, so that

$$p(D\,|\,a) \simeq \frac{1}{N_s} \prod_{\mathrm{bins}} \sum_{\mathrm{samples}} \exp\left[-\frac{1}{2} \sum_{\langle ij \rangle} \frac{\alpha_{ij}^2}{\sigma_{ij}^2} \right], \tag{8}$$

where N_s is the number of Monte–Carlo realisations of the data. Using this procedure, we find $a = 5.21 \pm 0.66\,\mathrm{kpc}$. Figure 4 depicts

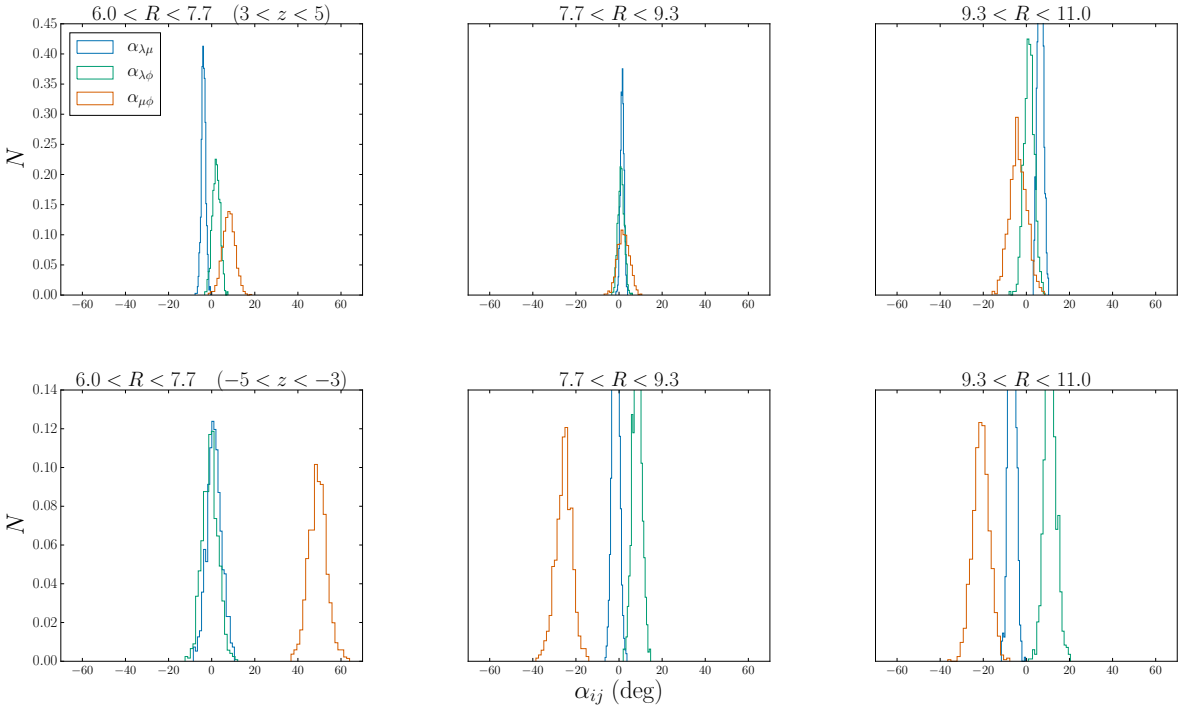

Figure 5. The distribution of spheroidal tilt angles given our best fit value of $a = 5.21$ kpc, $\alpha_{\lambda\mu}$ (blue), $\alpha_{\lambda\phi}$ (green) and $\alpha_{\mu\phi}$ (red) in degrees at 6 equally spaced locations in Galactocentric cylindrical polars (R, z) with $6 \leq R \leq 11$ kpc and $3 \leq |z| \leq 5$ kpc. Written above each plot is the position of the centroid of the bin in question. A summary of these distributions can be found in Table 3.

the likelihood distribution of the focal distance, as well as the distribution of the data with respect to the best–fit coordinate system. Having discovered the optimal focal distance for this data, we then performed the same analysis in this coordinate system as we did for the spherical coordinates. Figure 5 depicts the Monte–Carlo distributions of the tilt angles, and Table 3 gives the mean and variance of each tilt angle in each spatial bin. When the best–fit a is used, we find marginally better alignment with the prolate spheroidal coordinates than with spherical coordinates. The same issues are noted below the plane, where significant deviations from alignment are detected.

2.2.3 *Symmetry of the velocity distributions*

Another matter of interest is the symmetry of the velocity distributions under the transformation $\boldsymbol{v} \to -\boldsymbol{v}$. If the DF of the stellar halo depends only on integrals of motion that are even in the velocities, then the velocity distribution is completely symmetric and the means $\langle v_r \rangle$, $\langle v_\theta \rangle$, $\langle v_\phi \rangle$ all vanish. In fact, there is some evidence for rotating components in the halo (e.g., Carollo et al. 2007; Deason et al. 2011), albeit not clear-cut nor uncontroversial (e.g., Agnello & Evans 2012; Fermani & Schönrich 2013). Patchy streaming motions may be the result of localised coherent substructure.

For each velocity component, and in each bin, we compare the distribution of positive velocities with that of negative velocities using a Kolmogorov-Smirnov (KS) test to assess whether they are drawn from the same underlying distribution. Figure 6 depicts the cumulative distributions in each bin for a single Monte Carlo realisation of our dataset, along with the KS probability assigned for that particular bin and realisation. The KS test measures the supremum of the set of distances between the two CDFs being compared, such that two distributions with a large maximal separation are assigned a low KS probability.

We compute many Monte Carlo realisations of the data and from these compute the distributions of the KS probability for each velocity component in each bin. If the underlying distribution is symmetric, we expect the distribution of KS probabilities from many samples to be flat between 0 and 1. Each sample is divided into positive and negative observations and a KS test is performed. When this analysis is performed on the data, we see mostly flat distributions, save for in a couple of bins. Table 4 gives the median values of the KS probabilities for each velocity component in each bin. If the distribution is flat, we expect the median probability to be ~ 0.5, so significant deviations from this value suggest a skewed distribution. This is only the case in two of the low–latitude bins, where the v_ϕ distribution is inferred to be very asymmetric ($p \sim 0.01$). Some of this may be due to the effects of thick disk contamination. Another possibility is that the parts of the stellar halo closest to the disk are composed of some rotating populations.

3 SPHERICAL ALIGNMENT

Motivated by our analysis of the stellar halo, let us assume that the velocity ellipsoid is aligned with the spherical polar coordinate system. This means that all the cross terms $\langle v_r v_\theta \rangle = \langle v_r v_\phi \rangle = \langle v_\theta v_\phi \rangle$ vanish. The DF depends on phase space coordinates and so may have the completely general form $F(\boldsymbol{v}, \boldsymbol{x}) = F(v_r, v_\theta, v_\phi, r, \theta, \phi)$.

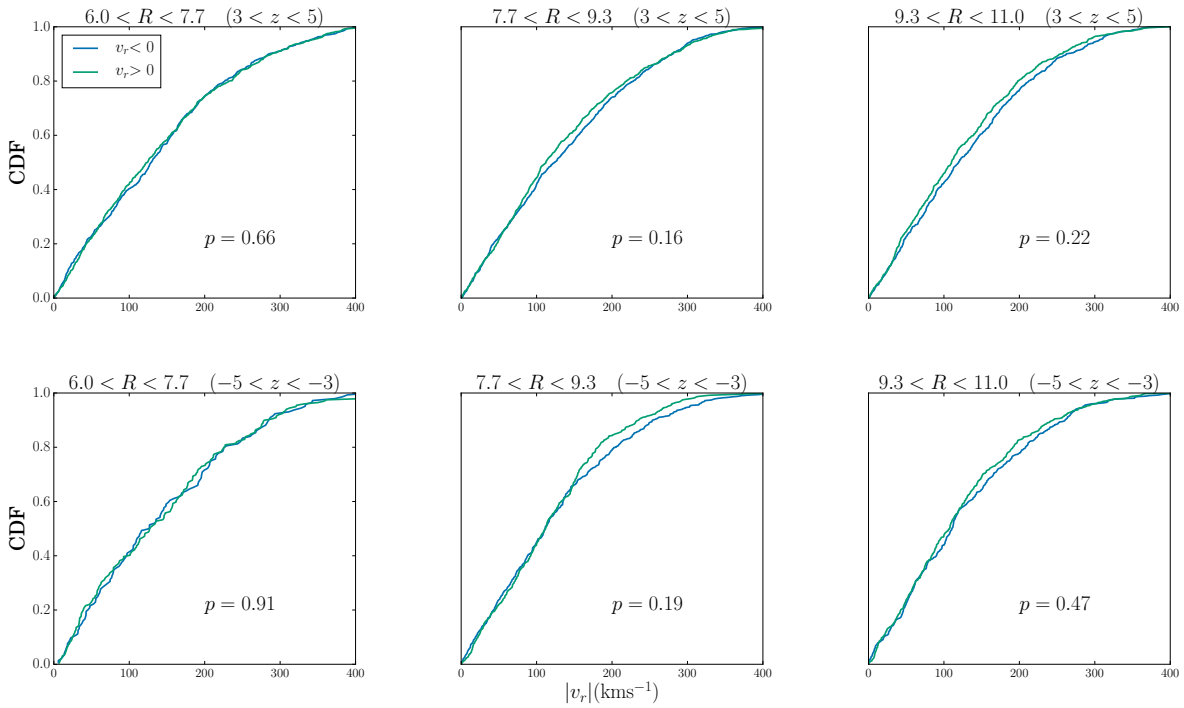

Figure 6. Cumulative radial velocity distributions of a single Monte Carlo realisation of our halo sample. The blue/green lines are CDFs stars with negative/positive v_r. Above each plot is the position of the centroid of the bin in kpc and inset is the KS probability that the two samples are drawn from the same underlying distribution. The KS probability measures the supremum of the set of distances between the two CDFs. A low KS probability is assigned if the supremum of the distances is large.

However, the DF is an integral of motion by Jeans Theorem, and so the Poisson bracket $\{F(\boldsymbol{v},\boldsymbol{x}), H\}$ must vanish. Under time reversal, integrals of motion remain integrals of motion, so the Poisson bracket $\{F(-\boldsymbol{v},\boldsymbol{x}), H\}$ must also vanish. Therefore, we can always construct the even function $F_{\rm e} = \frac{1}{2}[F(\boldsymbol{v},\boldsymbol{x}) + F(-\boldsymbol{v},\boldsymbol{x})]$, which must depend on even powers of the velocities. This is of course just the even part of the DF.

The even part of the DF may contain terms like $v_r^l v_\theta^m v_\phi^n$ provided $l + m + n$ is itself even. However, the cross-terms $\langle v_r v_\theta\rangle = \langle v_r v_\phi\rangle = \langle v_\theta v_\phi\rangle$ must all vanish at every position. On the grounds of naturalness, we expect that the DF must be of form $F_{\rm e} = F_{\rm e}(v_r^2, v_\theta^2, v_\phi^2, r, \theta, \phi)$ and so it must depend only on even powers of the velocity components in the aligned coordinate system. This is a key step in the proof, and the general conditions under which it is true can be made formal and explicit, albeit with some effort (An & Evans 2015). However, here we can appeal directly to the data – we have shown in the preceding section that the velocity distributions of the stellar halo are symmetric under the transformations $v_r \to -v_r$ or $v_\theta \to -v_\theta$ or $v_\phi \to -v_\phi$. In other words, without changing the underlying potential, we can always construct the even part of the DF, which must depend on even powers only of the individual velocity components. Smith et al. (2009a) reached the same conclusion that the DF may be chosen to depend only on even powers, but their line of reasoning was incorrect.

Introducing canonically conjugate momenta $p_r = v_r$, $p_\theta = r v_\theta$ and $p_\phi = r\sin\theta v_\phi$ (Landau & Lifshitz 1976), then the Hamiltonian is

$$H = \frac{1}{2}\Big(p_r^2 + \frac{p_\theta^2}{r^2} + \frac{p_\phi^2}{r^2\sin^2\theta}\Big) - \psi(r,\theta,\phi), \tag{9}$$

where ψ is the gravitational potential. Without loss of generality, the DF can now be recast as $F_{\rm e}(H, p_\theta^2, p_\phi^2, r, \theta, \phi)$ by using the Hamiltonian to eliminate p_r^2. The Poisson bracket $\{F_{\rm e}, H\}$ must vanish. The H in the DF may be treated as a constant when evaluating the derivatives in the Poisson bracket, yielding:

$$p_r\frac{\partial F}{\partial r} + \frac{p_\theta}{r^2}\frac{\partial F}{\partial\theta} + \frac{p_\phi}{r^2\sin^2\theta}\frac{\partial F}{\partial\phi} + \left(\frac{p_\phi^2\cos\theta}{r^2\sin^3\theta} + \frac{\partial\psi}{\partial\theta}\right)\frac{\partial F}{\partial p_\theta} + \frac{\partial\psi}{\partial\phi}\frac{\partial F}{\partial p_\phi} = 0 \tag{10}$$

The first term is antisymmetric in p_r, whereas all other terms are symmetric. So, it must be the case that F does not depend on r. (This is analogous to the elimination of the nodes in the N-body problem which similarly reduces the order of the system in phase space by two – see e.g., Boccaletti & Pucacco (1996).)

We now multiply by r^2 and differentiate with respect to r at constant $H, p_\theta, p_\phi, \theta, \phi$ to obtain:

$$\frac{\partial F}{\partial p_\theta}\frac{\partial^2}{\partial r\partial\theta}\left(r^2\psi\right) + \frac{\partial F}{\partial p_\phi}\frac{\partial^2}{\partial r\partial\phi}\left(r^2\psi\right) = 0 \tag{11}$$

The first term is odd with respect to p_θ, the second term odd with respect to p_ϕ. However, the equation must remain true under $p_\phi \to -p_\phi$ or $p_\theta \to -p_\theta$, and so each term must separately vanish.

There are four possibilities – either (case i)

$$\frac{\partial F_{\rm e}}{\partial p_\phi} = 0 = \frac{\partial F_{\rm e}}{\partial p_\theta}, \tag{12}$$

or case (ii)

$$\frac{\partial F_{\rm e}}{\partial p_\theta} = 0 = \frac{\partial^2}{\partial r \partial \phi}\left(r^2\psi\right), \tag{13}$$

or case (iii)

$$\frac{\partial F_{\rm e}}{\partial p_\phi} = 0 = \frac{\partial^2}{\partial r \partial \theta}\left(r^2\psi\right), \tag{14}$$

or case (iv)

$$\frac{\partial^2}{\partial r \partial \phi}\left(r^2\psi\right) = 0 = \frac{\partial^2}{\partial r \partial \theta}\left(r^2\psi\right), \tag{15}$$

Cases (i)-(iii) lead to the degenerate cases in which two or three of the semiaxes of the velocity ellipsoid are the same. For example, case (i) tells us that $F_{\rm e}$ is independent of both p_θ and p_ϕ. On returning to eq (10), we see that it also follows that $F_{\rm e}$ is independent of the conjugate coordinates θ and ϕ as well, leaving us with $F_{\rm e} = F_{\rm e}(H)$, or solutions with completely isotropic velocity ellipsoids. The other degenerate cases are when the DF is given by $F_{\rm e} = F_{\rm e}(H, |\boldsymbol{L}|)$ in a spherical potential, or $F_{\rm e} = F_{\rm e}(E, L_z)$ in an axisymmetric potential. Here, $\boldsymbol{L}$ is the angular momentum, whilst L_z is the component of $\boldsymbol{L}$ that is parallel to the symmetry axis. Both lead to the velocity ellipsoid possessing axial symmetry – in the former case with $\langle v_\theta^2\rangle = \langle v_\phi^2\rangle$, in the latter case with $\langle v_r^2\rangle = \langle v_\theta^2\rangle$. These models have been known since at least the Adams Prize essay of James Jeans (1919). However, it has also long been known that the velocity ellipsoid of Milky Way halo stars is triaxial with $\langle v_r^2\rangle > \langle v_\phi^2\rangle > \langle v_\theta^2\rangle$ (see e.g., Woolley 1978; Chiba & Beers 2000; Kepley et al. 2007; Smith et al. 2009b; Bond et al. 2010). Therefore, the degenerate instances of spherical alignment do not seem to apply to the case of the Milky Way stellar halo anyhow.

Only case (iv) survives. The solution to $\partial^2(r^2\psi)/\partial r\partial\theta = 0$ is

$$r^2\psi = A(r,\phi) + B(\theta,\phi), \tag{16}$$

where $A(r,\phi)$ and $B(\theta,\phi)$ are arbitrary functions of the indicated arguments. If we also demand that $\partial^2(r^2\psi)/\partial r\partial\phi = 0$, then we have

$$\frac{\partial^2 A}{\partial r\partial\phi} = 0 \implies A = A_1(r) + A_2(\phi), \tag{17}$$

where $A_1(r)$ and $A_2(\phi)$ are again arbitrary. Thus absorbing A_2 into a new function $A_3(\theta,\phi)$, we obtain the result

$$\psi = \frac{A_1(r)}{r^2} + \frac{A_2(\theta,\phi)}{r^2} = \psi_1(r) + \frac{A_2(\theta,\phi)}{r^2}, \tag{18}$$

where $\psi_1(r) = A_1(r)/r^2$ and $A_2(\theta,\phi)$ is an arbitrary function. So, the radial coordinate separates from the other coordinates. This means that there is an additional integral of the motion by separation of the Hamilton-Jacobi equation:

$$I = \frac{1}{2}\left(p_\theta^2 + \frac{p_\phi^2}{\sin^2\theta}\right) - A_2(\theta,\phi). \tag{19}$$

So, we can additionally replace p_θ^2 with I in the DF, which means that $F_{\rm e} = F_{\rm e}(H, I, p_\phi^2, r, \theta, \phi)$. Taking the Poisson bracket and exploiting the fact that both H and I may be taken as constants during the differentiation, we deduce that $F_{\rm e}$ must now be independent of both r and θ, and so are just left with

$$\frac{p_\phi}{r^2\sin^2\theta}\frac{\partial F_{\rm e}}{\partial\phi} + \frac{\partial\psi}{\partial\phi}\frac{\partial F_{\rm e}}{\partial p_\phi} = 0 \tag{20}$$

Multiplying through by $\sin^2\theta$ and differentiating with respect to θ gives

$$\frac{\partial}{\partial\theta\partial\phi}\left(\sin^2\theta\,\psi\right) = 0. \tag{21}$$

Inserting eq. (18) into eq. (21), this leads to the separable or Stäckel potential in spherical polars, namely

$$\psi = \psi_1(r) + \frac{\psi_2(\theta)}{r^2} + \frac{\psi_3(\phi)}{r^2\sin^2\theta}, \tag{22}$$

where $\psi_2(\theta)$ and $\psi_3(\phi)$ are arbitrary functions. This is the result claimed by Smith et al. (2009a); namely, that if the velocity ellipsoid is aligned everywhere in spherical polar coordinates, then the only non-singular potential is spherically symmetric. It is worth emphasizing the very general nature of the assumptions required to deduce the result. *Nothing about the quadratic nature of the integrals or the separability of the underlying potential has been assumed. Rather, these are logical consequences that follow from the assumption of spherical alignment.* This proof follows the outline of the one presented in Smith et al. (2009a), amplifying the working where necessary. It differs in one respect. Smith et al. (2009a) assumed that $\langle v_r\rangle = 0$ implies that the DF depends on v_r^2. This though is not necessarily true.

Note too that for the purposes of the theorem it is immaterial whether the population self-consistently generates the gravitational field or not. The result holds good for tracer populations moving in an externally imposed potential, as well as populations that generate the gravity field in which they move. Finally, although the singularities in the potentials (18) or (22) at $r = 0$ may seem objectionable, we show in Appendix A that this awkwardness can sometimes be avoided.

4 OTHER ALIGNMENTS

Other alignments of the velocity ellipsoid are also of interest in galactic astronomy and dynamics. Here, we consider cylindrical and spheroidal alignment in some detail. From our work on spherical alignment, we may conjecture that the only possible solutions for triaxial velocity ellipsoids are the separable or Stäckel potentials. We now demonstrate that such is indeed true.

4.1 Cylindrical Alignment

This case is interesting because it has has direct implications for the popular JAM models introduced by Cappellari (2008), which assume cylindrical alignment. In JAM, the only non-vanishing components of the velocity dispersion tensor are $\langle v_R^2\rangle$, $\langle v_\phi^2\rangle$ and $\langle v_z^2\rangle$. JAM models assume a fixed anisotropy $\beta_z = \langle v_z^2\rangle/\langle v_R^2\rangle$. Using the boundary conditions that the velocity dispersions vanish at infinity then leads to an elegant way of solving the Jeans equations for the velocity dispersion as quadratures.

We take as our starting point the fact that the velocity ellipsoid is aligned with the cylindrical polar coordinate system so that all the cross terms $\langle v_R v_\phi\rangle = \langle v_z v_\phi\rangle = \langle v_R v_z\rangle$ vanish. As before, we can take the even part of the DF to be $F_{\rm e} = F_{\rm e}(p_R^2, p_\phi^2, p_z^2, r, \phi, z)$, where the canonically conjugate momenta are $p_R = v_R$, $p_\phi = Rv_\phi$ and $p_z = v_z$. The Hamiltonian is

$$H = \frac{1}{2}\left(p_R^2 + \frac{p_\phi^2}{R^2} + p_z^2\right) - \psi(R,\phi,z), \tag{23}$$

where ψ is the gravitational potential. The even part of the DF can now be recast as $F_{\rm e}(p_R^2, p_\phi^2, H, R, \phi, z)$ by using the Hamiltonian to eliminate p_z^2. The H in the DF may be treated as a constant when evaluating the derivatives in the Poisson bracket, yielding:

$$p_R\frac{\partial F_{\rm e}}{\partial R} + \frac{p_\phi}{R^2}\frac{\partial F_{\rm e}}{\partial\phi} + p_z\frac{\partial F_{\rm e}}{\partial z} + \left(\frac{p_\phi^2}{R^3} + \frac{\partial\psi}{\partial R}\right)\frac{\partial F_{\rm e}}{\partial p_R} + \frac{\partial\psi}{\partial\phi}\frac{\partial F_{\rm e}}{\partial p_\phi} = 0 \tag{24}$$

As only the third term involves p_z, it follows that $\partial F_{\rm e}/\partial z = 0$ and so $F_{\rm e}$ must also be independent of z. Now differentiate with respect to z to obtain

$$\frac{\partial F_{\rm e}}{\partial p_R}\frac{\partial^2 \psi}{\partial R \partial z} + \frac{\partial F_{\rm e}}{\partial p_\phi}\frac{\partial^2 \psi}{\partial \phi \partial z} = 0 \tag{25}$$

The first term is odd with respect to p_R, the second term odd with respect to p_ϕ. Hence, for this to be generally true, each term must separately vanish.

There are again four possibilities – either (case i)

$$\frac{\partial F_{\rm e}}{\partial p_R} = 0 = \frac{\partial F_{\rm e}}{\partial p_\phi}, \tag{26}$$

or case (ii)

$$\frac{\partial F_{\rm e}}{\partial p_R} = 0 = \frac{\partial^2 \psi}{\partial \phi \partial z}, \tag{27}$$

or case (iii)

$$\frac{\partial F_{\rm e}}{\partial p_\phi} = 0 = \frac{\partial^2 \psi}{\partial R \partial z}, \tag{28}$$

or case (iv)

$$\frac{\partial^2 \psi}{\partial \phi \partial z} = 0 = \frac{\partial^2 \psi}{\partial R \partial z} \tag{29}$$

As before, cases (i) - (iii) provide the degenerate solutions in which one or more of the velocity dispersions is everywhere the same. This leaves case (iv), which is non-degenerate and $\langle v_R^2 \rangle$, $\langle v_\phi^2 \rangle$ and $\langle v_z^2 \rangle$ are all unequal, as the general case. Solving $\partial^2 \psi / \partial \phi \partial z = 0$ is

$$\psi = A(R, \phi) + B(R, z), \tag{30}$$

where $A(R, \phi)$ and $B(R, z)$ are arbitrary functions of the indicated arguments. When we also demand that $\partial^2 \psi / \partial R \partial z = 0$, then we have

$$\psi(R, \phi, z) = A(R, \phi) + \psi_3(z), \tag{31}$$

where $\psi_3(z)$ is an arbitrary function. Notice that we have now proved that the z component separates from the other coordinates, and that the energy in the z direction H_z

$$H_z = \frac{1}{2}p_z^2 - \psi_3(z), \tag{32}$$

is an integral of motion.

Of course, we can now repeat our calculation by recasting the even part of the DF as $F_{\rm e}(H, p_\phi^2, H_z, R, \phi, z)$ using the Hamiltonian H to eliminate p_R^2 and H_z to eliminate p_z^2. Again taking the Poisson bracket $\{F_{\rm e}, H\} = 0$, we straightforwardly establish that $F_{\rm e}$ must be independent of the conjugate coordinates R and z, and are left with

$$\frac{p_\phi}{R^2}\frac{\partial F_{\rm e}}{\partial \phi} + \frac{\partial \psi}{\partial \phi}\frac{\partial F_{\rm e}}{\partial p_\phi} = 0. \tag{33}$$

Multiplying through by R^2 and differentiating with respect to R gives

$$\frac{\partial (R^2 \psi)}{\partial R \partial \phi} = 0. \tag{34}$$

So, using eq (31), the final solution for the potential is

$$\psi = \psi_1(R) + \frac{\psi_2(\phi)}{R^2} + \phi_3(z), \tag{35}$$

where $\psi_1(R)$ and $\psi_2(\phi)$ are arbitrary. This is the separable or Stäckel potential in cylindrical polars (see e.g., Landau & Lifshitz 1976; Goldstein 1980).

Of course, it has long been known that if the potential is separable in cylindrical polars, then the velocity ellipsoid is aligned in the cylindrical polar coordinate system. What has been proved here for the first time is the converse. If the velocity ellipsoid is non-degenerate and aligned in cylindrical polar coordinates, then the gravitational potential is separable or Stäckel in cylindrical polar coordinates. The degenerate cases are the ones in which at least two of the semiaxes are everywhere the same, and so correspond to models with DFs that have $F(E)$ (isotropic DFs), $F(E, L_z)$ (axisymmetric potential) and $F(E, E_z)$ (translationally invariant potential).

What then is the status of the JAM models of Cappellari (2008)? The Jeans solutions are cylindrically aligned with (in general) three unequal axes. The only such physical models must have potentials that separate in the cylindrical polar coordinate system. Unfortunately, this yields through Poisson's equation a total matter density of the form

$$\rho(R, \phi, z) = \rho_1(R) + \frac{\rho_2(\phi)}{R^4} + \rho_3(z). \tag{36}$$

The fact that the density separates into stratified layers in z with the same profile in (R, ϕ) makes this unrealistic for all known astrophysical objects. Reluctantly, we must conclude that for arbitrary and astrophysically realistic potentials, the JAM models are all unphysical (i.e., do not have an underlying DF).

We advocate exercising considerable care in the use of JAM solutions, not least because the alignment also seems unnatural (except perhaps in the central parts of elliptical galaxies). Physically, we expect astrophysical objects to be at least roughly aligned in spherical polar coordinates rather than cylindrical, as is borne out by our investigations of the stellar halo. Probably, it makes sense to use the JAM solutions for preliminary models only before they are elaborated upon with Schwarzschild (Schwarzschild 1979) or Made-To-Measure methods (Syer & Tremaine 1996; Dehnen 2009).

4.2 Spheroidal Alignment

It is straightforward to generalize the proof to the instance of axisymmetric stellar systems with velocity dispersions aligned in spheroidal coordinates (λ, μ, ϕ). This coordinate system has been introduced in eq. (5) and is described in detail in, for example, Morse & Feshbach (1953) or Binney & Tremaine (2008). Here, we will show that if the velocity ellipsoid is everywhere aligned in spheroidal coordinates ($\langle v_\lambda v_\phi \rangle = \langle v_\lambda v_\mu \rangle = \langle v_\mu v_\phi \rangle = 0$), then the gravitational potential has Stäckel or separable form. Again, we construct the even part of the DF. Introducing canonical coordinates, the DF has the form $F_{\rm e}(p_\lambda^2, p_\mu^2, p_\phi^2, \lambda, \mu, \phi)$. The Hamiltonian is

$$H = \frac{1}{2}\Big(\frac{p_\lambda^2}{P^2} + \frac{p_\mu^2}{Q^2} + \frac{p_\phi^2}{R^2}\Big) - \psi(\lambda, \mu, \phi), \tag{37}$$

where the scale factors are P, Q and R are

$$\begin{aligned} P^2 &= \frac{\lambda - \mu}{4(\lambda + a)(\lambda + b)}, \qquad Q^2 = \frac{\mu - \lambda}{4(\mu + a)(\mu + b)}, \\ R^2 &= \frac{(\lambda + a)(\mu + a)}{a - b}, \end{aligned} \tag{38}$$

and a and b are constants (see for example the Tables of Lynden-Bell (1962) or eq (6) of Evans & Lynden-Bell (1989) or Section 2 of de Zeeuw (1985)). This implies that the DF can be re-written as $F_{\rm e}(H, p_\mu^2, p_\phi^2, \lambda, \mu, \phi)$ Just as before, requiring the Poisson bracket $\{H, F_{\rm e}\}$ to vanish implies that $\partial F_{\rm e}/\partial \lambda$ also vanishes and so $F_{\rm e}$ is

independent of λ. This leaves us with the condition:

$$A\frac{\partial F_{\rm e}}{\partial p_\mu} - \frac{\partial \psi}{\partial \phi}\frac{\partial F_{\rm e}}{\partial p_\phi} = \frac{p_\mu}{Q^2}\frac{\partial F_{\rm e}}{\partial \mu} + \frac{p_\phi}{R^2}\frac{\partial F_{\rm e}}{\partial \phi} \tag{39}$$

with

$$A = \frac{1}{\lambda-\mu}\left[\frac{p_\mu^2}{2}\frac{\partial}{\partial \mu}\left(\frac{\lambda-\mu}{Q^2}\right) + \frac{p_\phi^2}{2}\frac{\partial}{\partial \mu}\left(\frac{\lambda-\mu}{R^2}\right) - \frac{\partial}{\partial \mu}\left((\lambda-\mu)\psi\right) + H\right]. \tag{40}$$

Again, the equation must hold on transforming $p_\mu \rightarrow -p_\mu$, so that in the general case (i.e., ignoring degenerate cases like isotropy), we must have

$$A\frac{\partial F_{\rm e}}{\partial p_\mu} = \frac{p_\mu}{Q^2}\frac{\partial F_{\rm e}}{\partial \mu}, \qquad \frac{\partial \psi}{\partial \phi}\frac{\partial F_{\rm e}}{\partial p_\phi} = \frac{p_\phi}{R^2}\frac{\partial F_{\rm e}}{\partial \phi}. \tag{41}$$

Multiplying the first equation by $\lambda - \mu$, differentiating with respect to λ at constant H and then using the definitions of the scale factors gives us the simple result

$$\frac{\partial^2}{\partial \lambda \partial \mu}\left((\lambda-\mu)\psi\right) = 0. \tag{42}$$

Integrating up, this gives us

$$\psi = \frac{A(\lambda,\phi) - B(\mu,\phi)}{\lambda-\mu}, \tag{43}$$

where $A(\lambda,\phi)$ and $B(\mu,\phi)$ are arbitrary.

Now, we can return to the beginning and instead of eliminating p_λ^2 in terms of H, we can eliminate p_ϕ^2 so that the DF is $F_{\rm e}(p_\lambda^2, p_\mu^2, H, \lambda, \mu, \phi)$. Repeating the steps gives us

$$\frac{\partial^2}{\partial \lambda \partial \phi}\left(R^2\psi\right) = \frac{\partial^2}{\partial \mu \partial \phi}\left(R^2\psi\right) = 0, \tag{44}$$

from which on inserting eq. (43), we obtain the separable or Stäckel potential in spheroidal coordinates

$$\psi = \frac{f_1(\lambda) - f_2(\mu)}{\lambda-\mu} + \frac{f_3(\phi),}{R^2}, \tag{45}$$

with $f_1(\lambda)$, $f_2(\mu)$ and $f_3(\phi)$ arbitrary functions of indicated arguments. Of course, these potentials have a long history in both classical mechanics (e.g., Levi-Civita 1904; Whittaker 1917; Weinacht 1924; Eisenhart 1934, 1948) and stellar dynamics (e.g., Eddington 1915; Clark 1937; Lynden-Bell 1962). In astrophysical applications, it is usual to set $f_3(\phi) = 0$ as otherwise the gravitational potential diverges on the axis $R = 0$. de Zeeuw (1985) provided examples – now known as the perfect oblate or prolate spheroids – of realistic self-gravitating stellar systems with density stratified on similar concentric spheroids that have a potential of Stäckel form. The models are important, as their orbital structure is generic (see e.g., Boccaletti & Pucacco 1996; Binney & Tremaine 2008).

It has been known for many years that, in the axisymmetric Stäckel potentials, the velocity ellipsoid is aligned in spheroidal coordinates (e.g., Lynden-Bell 1960; de Zeeuw 1985; Evans & Lynden-Bell 1989). We have shown here the converse also holds true. If the velocity ellipsoid is spheroidally aligned everywhere, then the potential must be of separable or Stäckel form.

Spherical polar, cylindrical polar and spheroidal coordinates are all limits of the most general case, ellipsoidal coordinates (Morse & Feshbach 1953). It may well be suspected that the theorem holds true for ellipsoidal coordinates as well. Such is indeed true, but we relegate details of this, the most cumbersome case, to Appendix B. Finally, it is also reasonable to suspect that a general proof can be found, irrespective of the coordinate system. In Appendix C, we show that just the assumption of a triaxial velocity ellipsoid aligned everywhere in some orthogonal coordinate system, together with the existence of a steady-state DF, is sufficient to constrain the system to be Stäckel in ellipsoidal coordinates (or one of its limits). Although this material has been placed in an Appendix as it is somewhat mathematical, nonetheless we regard it as an important, new, and more powerful, proof of Eddington's (1915) theorem which does not rest on the restrictive ellipsoidal hypothesis.

5 MADE-TO-MEASURE MODELS OF THE STELLAR HALO

Theorems on exact alignment are interesting, but in practice the alignment is approximate and the data extend only over high latitude fields that are comparatively nearby. Is it possible to build models in which the alignment is close to spherical, but the gravitational potential is flattened?

To investigate this, we use a made-to-measure method to construct a triaxial stellar halo tracer population in a potential generated by a triaxial NFW dark matter halo. We utilise the made-to-measure code of Dehnen (2009, hereafter D09). The construction of this model follows very closely the construction of the models presented in D09 and here we only briefly describe the made-to-measure method.

The made-to-measure technique was pioneered by Syer & Tremaine (1996). In their formulation, an equilibrium model is constructed by evolving an N-body simulation whilst simultaneously adjusting the particle weights until a merit function is optimized. The merit function is expressed as

$$Q = \mu S - \frac{1}{2}C, \tag{46}$$

where C is a cost function that quantifies the deviation of the model from our target model (for instance, the χ^2 difference between the model moments and the target moments) and S is an entropy term that regularizes the weight distribution of the particles. The N-body simulation is evolved whilst each particle weight w_i is adjusted according to a first-order differential equation that maximises the merit function Q. One difficulty encountered by Syer & Tremaine (1996) is that the cost function naturally fluctuates as the simulation is evolved due to Poisson noise, so some form of smoothing is required to ensure the algorithm converges. D09 pointed out that Syer & Tremaine's method of simply averaging the model properties used in the cost function did not ensure the model converged, so D09 instead proposed smoothing the merit function Q by making the weight-adjustment equation a second-order differential equation. Several other improvements to the original algorithm were presented by D09. In his formulation (i) each particle is evolved on its own dynamical timescale such that the outer parts of the model converge as rapidly as the inner regions, (ii) a total weight constraint is included as part of the merit function and (iii) the particles are resampled when the ratio between the minimum and maximum weight (normalized with respect to the priors) exceeds a chosen value. The last of these is implemented by, every so often, drawing new particles from the original set with probability proportional to their prior-normalized weights and adding a random velocity offset with a magnitude that declines exponentially as a function of the simulation time. For the model presented below we use very similar parameters for the algorithm as those presented in D09.

Using the made-to-measure method, we construct an equilibrium tracer stellar population inside a fixed dark matter potential. The density profile of both the dark matter and the tracer population

is given by a truncated double power law of the form

$$\rho_i \propto \left(\frac{q_i}{r_{0,i}}\right)^{-\gamma_i}\left[1+\left(\frac{q_i}{r_{0,i}}\right)\right]^{(\gamma_i-\beta_i)}\mathrm{sech}\left(\frac{q_i}{r_{t,i}}\right), \tag{47}$$

where $r_{0,i}$ is the scale radius of the ith component, r_t the truncation radius and the elliptical radius q is defined as

$$q_i^2 = \frac{x^2}{a_i^2}+\frac{y^2}{b_i^2}+\frac{z^2}{c_i^2}, \tag{48}$$

with $a_i b_i c_i = 1$. We choose the parameters for the NFW halo as $\gamma_{\rm NFW} = 1$, $\beta_{\rm NFW} = 3$, $(b/a)_{\rm NFW} = 0.9$, $(c/a)_{\rm NFW} = 0.8$, $r_{0,\rm NFW} = r_0$ and $r_{t,\rm NFW} = 10r_0$, whilst the target stellar halo has $\gamma_S = 1$, $\beta_{\rm S} = 4.5$, $(b/a)_{\rm S} = 0.8$, $(c/a)_{\rm S} = 0.6$, $r_{0,\rm S} = 1.73r_0$ and $r_{t,\rm S} = 9r_0$. These choices are motivated by several studies of the halo. In the dynamical models of Piffl et al. (2014), the NFW dark matter halo was found to have a scale radius of $r_0 = 15.5$ kpc, where the constraint comes mostly from the mass measurements of Wilkinson & Evans (1999) and the requirement that the halo lies on the mass-concentration relation. Deason et al. (2011) found from a population of BHB stars that the stellar halo had a scale radius of $r_{0,\rm S} = 27$ kpc and a flattening $(c/a)_{\rm S} = 0.59$. The axis ratios of the NFW profile are representative of those found in cosmological simulations (see for example Bryan et al. 2013).

The cost function corresponding to this density profile is given by

$$C_\rho = \sum_{\boldsymbol{n}}\left(\frac{A_{\boldsymbol{n}}-B_{\boldsymbol{n}}}{\sigma_{\boldsymbol{n}}}\right), \tag{49}$$

where $A_{\boldsymbol{n}}$ is the dot product of the model potential with the $\boldsymbol{n}^{th} = (n,l,m)^{\rm th}$ basis function of the Zhao (1996) basis set chosen to match the outer slope of the target model, and $B_{\boldsymbol{n}}$ is the corresponding target moment with $\sigma_{\boldsymbol{n}}$ an estimate of the error in the moment calculated from the variance of 100 realizations of the target model. We set $n_{\rm max} = 20$ and $l_{\rm max} = 12$ such that 588 moments are used to describe the density. Similarly, the potential used to describe the NFW halo is represented as a basis function expansion generated from a single sample of the density distribution. 10^6 particles were used for each realization of the stellar halo and 10^8 for realization of the dark matter density distribution. The total mass of the NFW halo is M and the stellar halo is treated purely as a tracer population.

Additionally, we impose an anisotropy profile for the tracer population as

$$\beta(q) = 1-\frac{\sigma_\theta^2+\sigma_\phi^2}{2\sigma_r^2} = \frac{\beta_0+\beta_\infty(q/r_0)}{1+(q/r_0)} \tag{50}$$

which goes from β_0 at small radii to β_∞ at large radii over a scale r_0. We choose $\beta_0 = 0$ and $\beta_\infty = 0.75$ which approximates the form for the anisotropy found by Williams & Evans (2015). The corresponding cost function C_β is the χ^2 deviation of the model anisotropy from the target calculated in elliptical shells with the same shape as the target density. The error is estimated as the Poisson noise arising from a measurement of the anisotropy from samples of an uncorrelated normal velocity distribution.

The initial N-body model is chosen to be the ergodic model with the required radial density profile, that is then flattened by the appropriate axis ratios and the velocities scaled to satisfy the tensor virial theorem. We began by running this model for 200 time units subject to the density constraints. The model converged within $\sim$ 50 time units and subsequent evolution with the weight adjustment switched off did not cause the model to deviate significantly from the target distribution. The anisotropy of this model was increased from weakly radial ($\beta \sim 0.2$) at $0.1r_0$ to more strongly radial ($\beta \sim 0.5$) at $r = r_{t,\rm S}$. We then proceeded to evolve the model further subject also to the anisotropy constraint. The model converged within $\sim$ 30 time units and again did not deviate from the target under subsequent evolution with no weight adjustment.

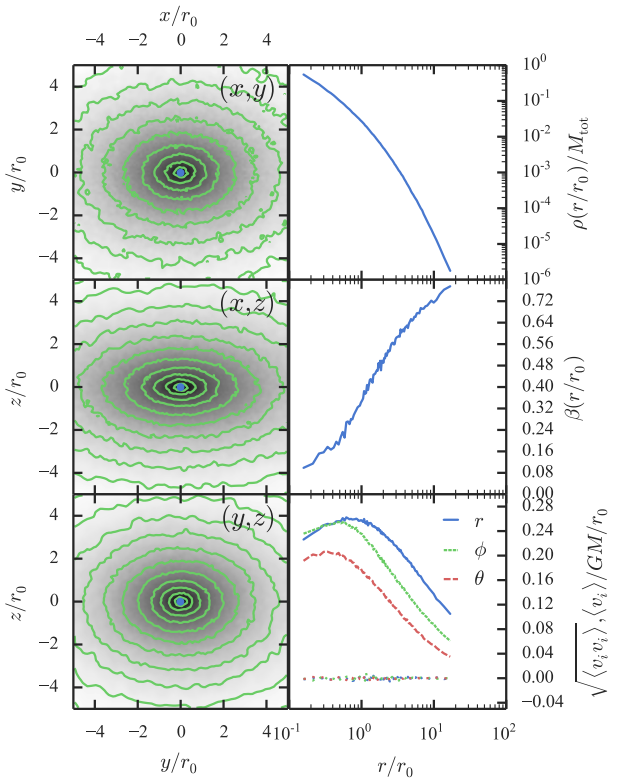

Figure 7. Made-to-measure stellar halo properties: the left panels show the density integrated along the line of sight in the three principal planes. The green contours are evenly spaced in logarithmic density and the blue point is the centre of mass. The top right panel shows the spherically-averaged density profile, the middle right panel the spherically-averaged anisotropy profile and the bottom right panel the spherically-averaged velocity dispersions and mean velocities. Note all the mean velocities are zero, as there is no net streaming.

The resulting simulation is plotted in Fig. 7. In Figures 8, 9 and 10, we show the velocity ellipses in the principal planes of the potential along with the misalignment from spherical alignment. In all three principal planes, the velocity ellipsoid is misaligned from spherical by $\lesssim 6$ degrees everywhere outside the scale radius of the stellar halo. Inside the scale radius, there are also large regions where the misalignment is $\lesssim 6$ degrees with the largest misalignments occurring at small x and small z as well as small x and small y. However, inspecting the velocity ellipses in these regions shows they are very round and so the misalignment measurement is more susceptible to shot noise. To inspect the impact of shot noise in the measurement of the tilt from the simulation we show α/σ_α in the (x,y) plane in Fig. **??**. σ_α was computed using propagation of errors from the measured dispersions. We see that the majority of the plane is consistent with being aligned within the shot noise. This plane is representative of the other two principal planes and similar to the simulations shown later. We conclude we are not dominated by shot noise from the simulation when drawing conclusions on the

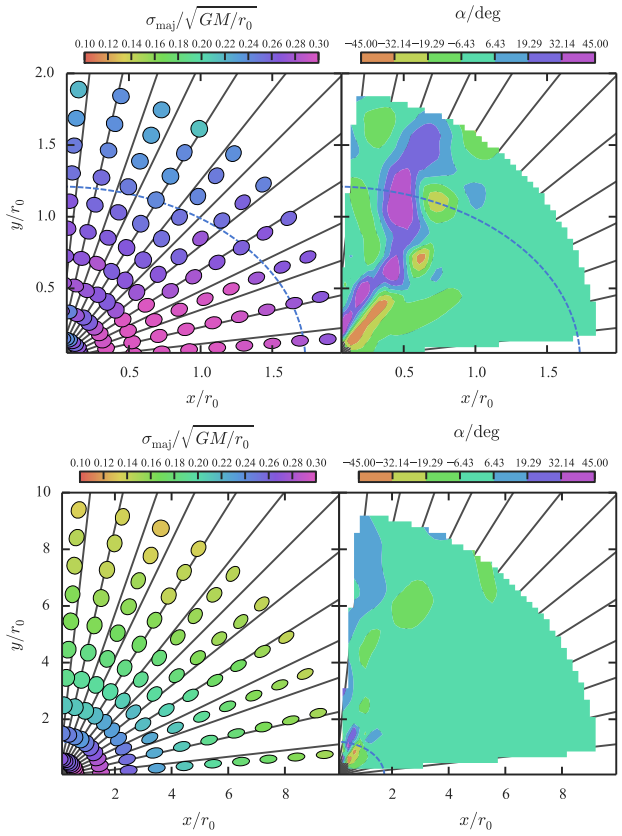

Figure 8. Tilt of the stellar halo for $(b/a)_{\rm NFW} = 0.9$, $(c/a)_{\rm NFW} = 0.8$ model in the (x, y) plane: the left panels show the velocity ellipses coloured by the magnitude of their major axis. The size of the ellipses is unimportant and chosen for ease of visualization. The black lines are radial. The right panels show the misalignment of the major axis of the ellipses from radial. The top two panels correspond to $0 \lesssim r/r_0 < 2$ whilst the lower two correspond to $0 \lesssim r/r_0 < 10$. In all panels the dotted blue line corresponds to $q_{\rm S} = r_{0,{\rm S}}$.

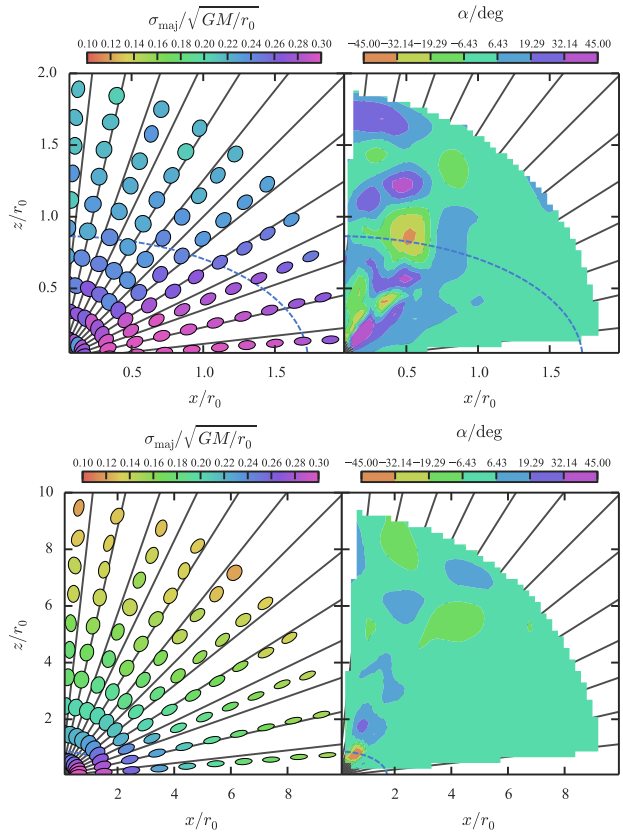

Figure 9. Tilt of the stellar halo for $(b/a)_{\rm NFW} = 0.9$, $(c/a)_{\rm NFW} = 0.8$ model in the (x, z) plane: see Fig. 8 for details.

degree of alignment. Instead when comparing these models with the data we are limited by the errors in the observational data.

For the simulation without the anisotropy constraint, we also found that there were large regions of spherical alignment particularly outside the scale radius in the (y, z) plane and along the x axis. However, near the y and z axis the ellipses became more circular with the suggestion that a minor axis is aligned with spherical polars. Increasing the anisotropy has the effect of increasing the volume in which the major axis of the velocity ellipsoid is spherically aligned. We are able to produce a realistic model of the stellar halo in a triaxial NFW halo that has a large volume in which that velocity ellipsoid is aligned with spherical polars within ~ 6 degrees.

The constructed model has a fairly round potential due to the only weakly triaxial NFW density profile for the dark matter. To investigate whether the alignment persists for a flatter model we now go on to construct a model with $(b/a)_{\rm NFW} = 0.7$, $(c/a)_{\rm NFW} = 0.5$, $(b/a)_{\rm S} = 0.65$ and $(c/a)_{\rm S} = 0.45$. All other parameters are kept the same. As expected, the region within which the alignment is less than $\sim$ 6 degrees has decreased compared to the rounder model but there are still considerable regions, particularly outside $q = r_S$, where the alignment is spherical. Finally, we report that we constructed a model with $(b/a)_{\rm NFW} = 1$, $(c/a)_{\rm NFW} = 0.1$, $(b/a)_{\rm S} = 1$ and $(c/a)_{\rm S} = 0.5$. This model has spherical alignment at very large radius ($q > 6r_S$) and within $q = r_S$ the long axis of the velocity ellipsoid is pointed more towards the plane for $R > z$ and the short axis is pointed more towards the plane for $z > R$. However, it should be reported that this model appears to be only marginally stable as the cost functions drift in time upon subsequent evolution of the made-to-measure code with no weight adjustment. Our models do not include the majority of the baryons in the Galaxy (i.e. the disc) but based on our constructed models we can make some predictions as to the effects. Including a disc will cause the velocity ellipses to tilt slightly towards the plane. However, at large distances the disc potential is dominated by the monopole component such that this effect will be small for the majority of the volume studied here. For example, both **?** and **?** find a flattening for the full potential of $q \sim 0.9$ when fitting the GD-1 stream which lies ~ 15 kpc from the Galactic centre so the models presented here are perhaps already too flattened *without* including the Galactic disc.

Notice that we did not introduce any requirement in the cost function (49) that drives the made-to-measure solutions to spherical alignment. We attempted to minimise the tilt angles from spherical alignment in spherical polar bins beyond a minimum elliptical radius but this produced no significant change to the structure of the models. It appears that the alignment cannot be significantly altered once the potential and tracer density have been specified. Making the models more radially anisotropic acts to make the alignment more obvious as the calculation of the tilt is less susceptible to Poisson noise. Flattened models with strong radial anisotropy seem to produce near-spherical alignment of the velocity ellipsoid in significant portions of configuration space without much difficulty. In

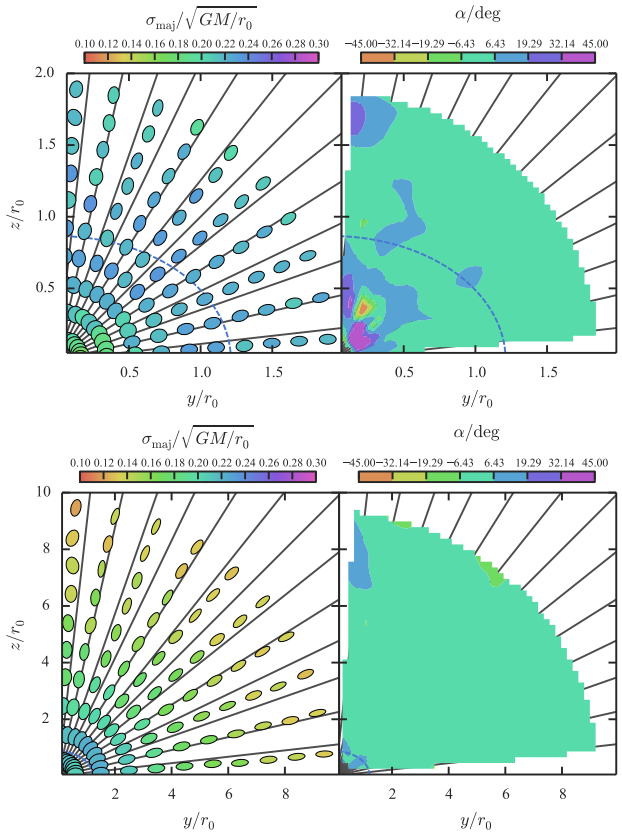

Figure 10. Tilt of the stellar halo for $(b/a)_{\rm NFW} = 0.9$, $(c/a)_{\rm NFW} = 0.8$ model in the (y, z) plane: see Fig. 8 for details.

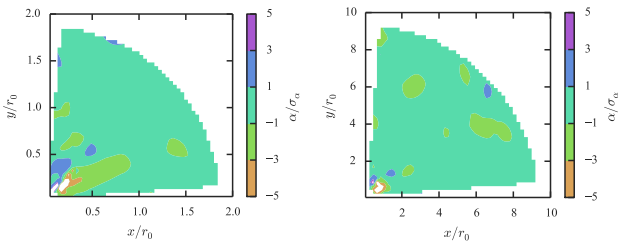

Figure 11. Tilt of the stellar halo divided by the error in the tilt for $(b/a)_{\rm NFW} = 0.9$, $(c/a)_{\rm NFW} = 0.8$ model in the (x, y) plane. The left panel shows a zoom-in of the right panel. The distributions in the other principal planes are very similar.

other words, the inferred alignment of the velocity ellipsoid in relatively small spatial volumes does not constrain the Galactic potential. Strong inferences can only made when global alignment is detected. Only with the advent of Gaia proper motions will we possess datasets of a large enough extent to use the velocity ellipsoid as a tool for inference on the symmetries of the Galactic matter distribution.

6 CONCLUSIONS

This paper has identified the circumstances under which the velocity dispersion tensor of a stellar system is everywhere aligned in

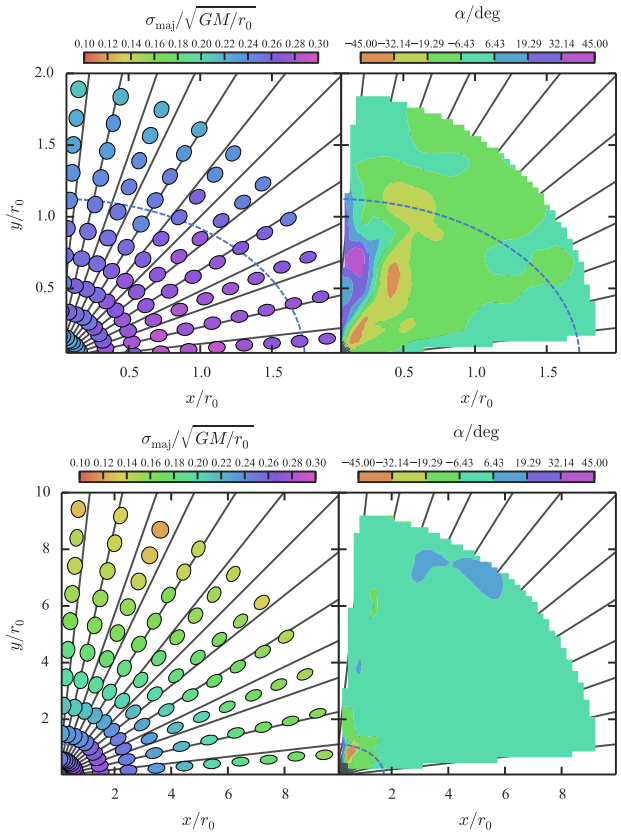

Figure 12. Tilt of the stellar halo tilt for flatter $(b/a)_{\rm NFW} = 0.7$, $(c/a)_{\rm NFW} = 0.5$ model in the (x, y) plane: see Fig. 8 for details.

the spherical polar coordinate system. Exact alignment in spherical polars is possible if (i) all three semiaxes are the same and the distribution function (DF) is isotropic, (ii) two of the semiaxes of the same ($\langle v_r^2 \rangle = \langle v_\theta^2 \rangle$) and the potential is axisymmetric with a DF depending on the energy E and angular momentum parallel to the symmetry axis L_z, (iii) all three semiaxes are in general different and the potential is of separable or Stäckel form in spherical polar coordinates. In the latter instance, if the potential is everywhere non-singular, then it must be spherically symmetric. Our proof is based on the ideas sketched out in Smith et al. (2009a).

We have shown that this theorem holds more generally. If the velocity ellipsoid of a stellar system is triaxial and points along orthogonal coordinate surfaces, then the potential must be of separable or Stäckel form in confocal ellipsoidal coordinates or one of its limits. The converse of this theorem – namely, if the potential is of Stäckel form then the velocity dispersion tensor aligns in the separable coordinate system – has been known since the time of Eddington (1915). *In our proof, we emphasise that no assumption has been made about the form of the DF, or the existence of integrals of the motion quadratic in the velocities.* Motivated by properties of the data on velocity distributions in the stellar halo, we have assumed relection symmetry in velocity space, although even this assumption can be relaxed (An & Evans 2015).

It is worth returning to Eddington's (1915) work on the ellipsoidal hypothesis to spell out the differences. Eddington postulated the existence of integrals of motion that are quadratic in the velocities. The ellipsoidal hypothesis is the statement that the DF depends on these integrals. Eddington then showed that the poten-

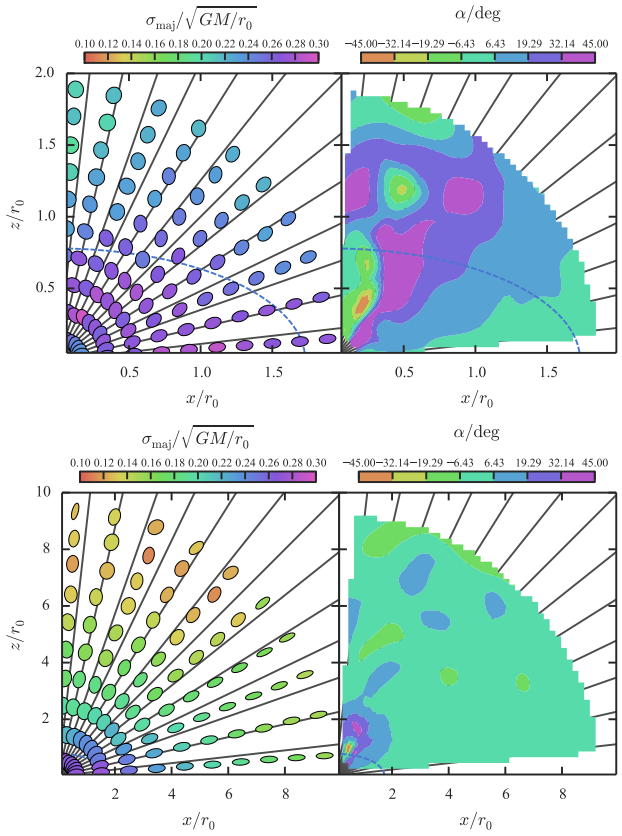

Figure 13. Tilt of the stellar halo for flatter $(b/a)_{\rm NFW} = 0.7$, $(c/a)_{\rm NFW} = 0.5$ model in the (x, z) plane: see Fig. 8 for details.

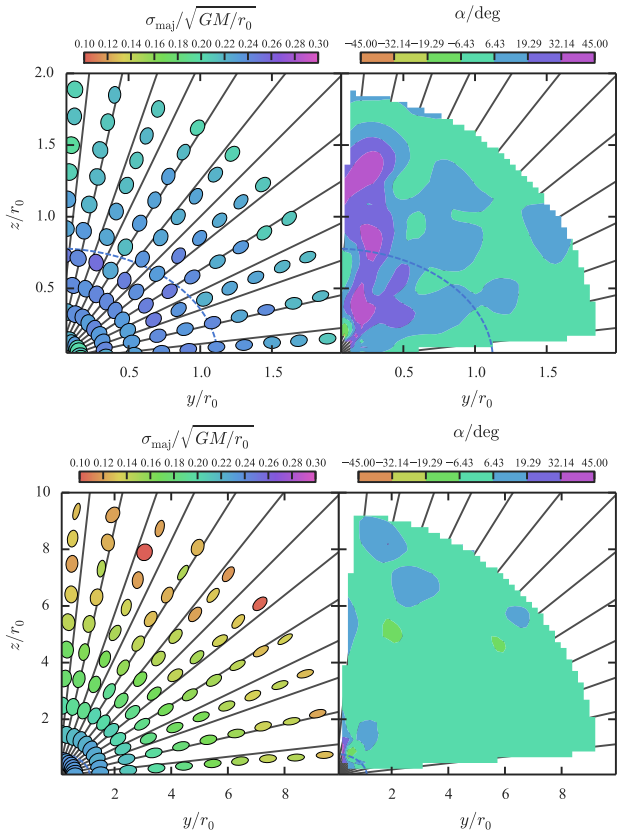

Figure 14. Tilt of the stellar halo tilt for flatter $(b/a)_{\rm NFW} = 0.7$, $(c/a)_{\rm NFW} = 0.5$ model in the (y, z) plane: see Fig. 8 for details.

tial has to be of separable or Stäckel form and the velocity ellipsoid diagonalises in the separating coordinates. However, integrals of the motion quadratic in the velocities only arise from separation of the Hamilton-Jacobi equation (see e.g., Makarov et al. 1967; Evans 1990). Hence, Eddington made an assumption of quadratic integrals that is tantamount to assuming the potential is of separable form in the first place.

One consequence of our theorem is that the elegant way of solving the Jeans equation for triaxial velocity ellipsoids using cylindrical polar alignment developed by Cappellari (2008) and known as "JAM modelling" only yields physical models if the potential is separable in the cylindrical polar coordinates. Unfortunately, this corresponds to total matter distributions that are unlike elliptical galaxies. If the potential is not of separable form in cylindrical polars, then there may be galaxy models with DFs that generate approximate cylindrical alignment, though this however remains to be demonstrated. JAM models may make good provisional starting points for constructing more realistic N-body or made-to-measure models, but they are not trustworthy on their own.

What then are the consequences for the stellar halo of the Milky Way? Our theorem applies to stellar systems in which the velocity ellipsoid is spherically or spheroidally aligned everywhere. The data on halo stars of the Milky Way do suggest it is aligned with the spherical polar coordinate system (to within 7°) for Galactocentric radii between $\sim$ 6 and $\sim$ 11 kpc in the Northern hemisphere. There are more substantial deviations in the Southern hemisphere, though this may be partly a consequence of the smaller size of the datasets. Alignment in prolate spheroidal coordinates (with a focal distance $a = 5.21 \pm 0.66$ kpc) gives a marginally better fit than spherical alignment, although deviations remain in the Southern hemisphere. In both calculations, no attempt has been made to remove substructure (such as Sagittarius stream stars or tidal debris) from the stellar halo sample. Such substructure is of course expected in ΛCDM and might spoil any exact alignment for an underlying smooth halo population.

Binney & McMillan (2011) have argued that only limited inferences on the potential may be drawn from the orientation of the velocity ellipsoid. They constructed DFs of the thin and thick disks of the Galaxy using orbital tori. They showed that at some locations above the plane in the vicinity of the Sun, the velocity ellipsoid is spherically aligned despite the matter distribution being highly flattened. However, the more recent data on the stellar halo provided by Bond et al. (2010) does provide a more substantial challenge. Now the alignment is known to be almost spherical over a large swathe of the Galaxy, and it is unclear whether flattened models exist that can provide this.

To understand whether such approximate alignment is consistent with flattened or triaxial potentials, we have used made-to-measure modelling (Syer & Tremaine 1996; Dehnen 2009). We constructed a triaxial stellar halo tracer model in an triaxial NFW dark matter potential. The tracer population was chosen to be more triaxial ($b/a = 0.8, c/a = 0.6$) than the NFW profile ($b/a = 0.9, c/a = 0.8$). The stellar halo was chosen to have a double power-law density profile and an anisotropy profile that went from isotropic at the centre to very radial in the outskirts. Despite the triaxiality of the potential, it was found that the velocity ellip-

soid had a major axis that deviated from spherical alignment by $\lesssim 6$ degrees for large regions of space. Outside the scale radius of the stellar halo, the velocity ellipsoid is nearly everywhere spherically aligned. We went on to investigate a model with a flatter NFW profile ($b/a = 0.7, c/a = 0.5$) and found that the volume of the spherical alignment region was decreased within the scale radius of the model although there were still considerable regions where the alignment was spherical.

If the alignment has to be exactly spherical everywhere, then the restriction on the potential is very severe. The potential has to be spherical if it is everywhere non-singular. However, if the alignment is only close to spherical over a substantial portion of configuration space, then a much greater variety of potentials are possible, including flattened ones. Strong inference on the potential can only be made if global spherical alignment is established. The Gaia satellite will provide six-dimensional phase space information for stars brighter than $V \approx 20$ within 20 kpc of the Sun. This may provide datasets of sufficient global coverage to enable the alignment of the velocity ellipsoid to be used as a tool for constraining the Galactic potential.

ACKNOWLEDGMENTS

NWE thanks Zeljko Ivezic for stimulating him to think about this matter again, as well as providing data files and advice on the propagation of errors. JLS acknowledges the use of the python package PYNBODY (Pontzen et al. 2013) for the visualization of N-body snapshots.

REFERENCES

Agnello A., Evans N. W. 2012, MNRAS, 422, 1767
Agnello A., Evans N. W., Romanowsky A. J. 2014, MNRAS, 442, 3284
An J. H., Evans N. W. 2011, MNRAS, 413, 1744
Arnold V. 1989, Mathematical Methods of Classical Mechanics, Springer Verlag
Arnold, R. 1995, MNRAS, 276, 293
Bacon R., Simien F., Monnet G., 1983, AA, 128, 405
Bacon R. 1985, AA, 143, 84
Binney J. 2014, MNRAS, 440, 787
Binney J., McMillan P. 2011, MNRAS, 413, 1889
Binney J., Merrifield M. 1998, Galactic Astronomy, (Princeton: Princeton University Press)
Binney J., Tremaine S. 2008, Galactic Dynamics, 2nd ed, (Princeton: Princeton University Press)
Boccaletti D., Pucacco G. 1996, Theory of Orbits 1: Integrable Systems and Non-Perturbative Methods, Springer Verlag, Berlin
Bond N. A., Ivezić, Ž., Sesar B., et al. 2010, ApJ, 716, 1
Bovy J., Rix H-W. 2013, ApJ, 779, 115
Bramich D. M., et al. 2008, MNRAS, 386, 887
Bryan S. E., Kay S. T., Duffy A. R., et al. 2013, MNRAS, 429, 3316
Cappellari M. 2008, MNRAS, 390, 71
Carollo D., Beers T. C., Leeg Y. S., et al. 2007, Nature, 450, 1020
Chandrasekhar S. 1942, Principles of Stellar Dynamics, Dover Publications
Chiba M., Beers T. C. 2000, AJ, 119, 2843
Clark, G. L. 1937, MNRAS, 97, 182
Deason A. J., Belokurov V., Evans N. W. 2011, MNRAS, 411, 1480
Deason A. J., Belokurov V., Evans N. W. 2011, MNRAS, 416, 2903
Dehnen, W., Gerhard, O. E. 1993, MNRAS, 261, 311
Dehnen W. 2009, MNRAS, 395, 1079
de Zeeuw T. 1985, MNRAS, 216, 273
Eddington A. S. 1915, MNRAS, 76, 37
Eisenhart L. P. 1934, Ann Math, 35, 284
Eisenhart L. P. 1948, Physical Review, 74, 87
Evans N. W. 1990, PRA, 41, 5666
Evans N. W. 2011, BASI, 39, 87
Evans N. W., Hafner R. M., de Zeeuw P. T. 1997, MNRAS, 286, 315
Evans N. W., Lynden-Bell D. 1989, MNRAS, 236, 801
Evans N. W., Bowden A. 2014, MNRAS, 443, 2
Evans N. W., An J., Bowden A., Williams A. A. 2015, MNRAS, 450, 846
Fermani F., Schönrich R. 2013, MNRAS, 432, 2402
Goldstein H. 1980 Classical Mechanics, Addison-Wesley
Hartmann M., Debattista V. P., Seth A., Cappellari M., Quinn T. R. 2011, MNRAS, 418, 2697
Hilbert D., Cohn-Vossen S. 1999, Geometry and the Imagination, Chelsea Publishing Company
Ivezić Ž., Sesar B., Jurić M., et al. 2008, ApJ, 684, 287
Jeans J.H. 1919, Problems of Cosmogony and Stellar Dynamics, Cambridge University Press, Cambridge
Kepley A. A, et al. 2007, AJ, 134, 1579
King III C., Brown W. R., Geller M. J., Kenyon S. J. 2015, arXiv:1506.05369
Landau L. D., Lifshitz E. M. 1976, Mechanics, Pergammon Press, Oxford
Levi-Civita T. 1904, Math Ann, 59, 383
Loebman S. R., Ivezić Ž., Quinn T. R., et al. 2014, ApJ, 794, 151
Lupton R. H., Gunn J. E. 1987, AJ, 93, 1106
Lynden-Bell D., 1960, PhD thesis, Cambridge University
Lynden-Bell D. 1962, MNRAS, 124, 95
Makarov A. A., Smorodinsky J. A., Valiev K., Winternitz P. 1967, Nuovo Cimento A Serie, 52, 1061
McDermid R. M., Alatalo K., Blitz L., et al. 2015, MNRAS, 448, 3484
Morse P., Feschbach H. 1953, Methods of Theoretical Physics, McGraw-Hill
Munn J. A., Monet D. G., Levine S. E., et al. 2004, AJ, 127, 3034
Piffl T., Binney J., McMillan P. J., et al. 2014, MNRAS, 445, 3133
Pontzen A., Roškar R., Stinson G., Woods, R. 2013, Astrophysics Source Code Library, 1305.002
Sanders J.L., Evans N.W. 2015, MNRAS, in press.
Schwarzschild, M. 1979, ApJ, 232, 236
Smith M. C., Evans N. W., An J. H. 2009a, ApJ, 698, 1110
Smith M. C., Evans N. W., Belokurov V., et al. 2009b, MNRAS, 399, 1223
Stäckel P. 1891, Uber die integration der Hamilton-Jacobischen Differentialgleichung mittels Separation der Variabelen, Habilitationsschrift, Halle
Syer D., Tremaine S. 1996, MNRAS, 282, 223
van der Marel R. P. 1994, MNRAS, 270, 271
van de Ven G., Hunter C., Verolme E. K., de Zeeuw P. T. 2003, MNRAS, 342, 1056
van de Ven G., Falcón-Barroso J., McDermid R. M., et al. 2010, ApJ, 719, 1481
Weinacht J. 1924, Math Ann, 91, 279

Whittaker E.T. 1917, Analytical Dynamics, Cambridge University Press
Wilkinson M. I., Evans N. W. 1999, MNRAS, 310, 645
Williams A. A., Evans N.W. 2015, MNRAS, in press.
Woolley R. 1978, MNRAS, 184, 311
Zhao H. 1996, MNRAS, 278, 488

APPENDIX A: EDDINGTON POTENTIALS WITHOUT TEARS

The separable potentials in spherical polars

$$\psi = \psi_1(r) + \frac{\psi_2(\theta)}{r^2} + \frac{\psi_3(\phi)}{r^2\sin^2\theta}, \tag{A1}$$

were introduced into stellar dynamics by Eddington. They are often called Eddington potentials in the astronomical literature (e.g., Clark 1937; Lynden-Bell 1962; Lupton & Gunn 1987). Astrophysically useful potentials must have $\psi_3(\phi) = 0$ to avoid singularities all along the polar axis.

The density then must have form

$$\rho = \rho_0(r) + \frac{g(\theta)}{r^4}. \tag{A2}$$

This may also seem objectionable as the density has a serious divergence at the origin. In fact, Eddington (1915) himself believed that $\psi_2(\theta) = 0$ and so $g(\theta) = 0$ for practical solutions. However, this is not the case, as the awkwardness can be avoided by requiring the non-spherical part of the density to fall like r^{-4} only outside the central region.

We now give a simple example of an axisymmetric density distribution that has such a property. We choose the density as

$$\rho(r,\theta) = \rho_0(r) + \rho_2(r)P_2(\cos\theta), \tag{A3}$$

where P_2 is the Legendre polynomial. For flattened systems with everywhere positive mass density, we need $\rho_2 \le 0$ and $\rho_0(r) + \rho_2(r) \ge 0$ for all $r > 0$. The gravitational potential of such systems is given by

$$\psi = \psi_0(r) + h(r)P_2(\cos\theta). \tag{A4}$$

where

$$\frac{\psi_0(r)}{4\pi G} = \frac{1}{r}\int_0^r r^2\rho_0(r)dr + \int_r^\infty \rho_0(r)dr \tag{A5}$$

and

$$\frac{5}{4\pi G}h(r) = \frac{1}{r^3}\int_0^r r^4\rho_2(r)dr + r^2\int_r^\infty \rho_2(r)\frac{dr}{r}, \tag{A6}$$

We wish to have $h \propto r^{-2}$ for $r \ge r_0$. In this region, we need to set $\rho_2(r) = \rho_2(r_0)(r_0/r)^4$ to ensure a continuous density.

We now define K to be

$$K = \int_0^{r_0}\left[r^4\rho_2(r) - r_0^4\rho_2(r_0)\right]dr \tag{A7}$$

and we evaluate our formula for h at $r > r_0$ to get

$$\frac{h(r)}{4\pi G} = \frac{K}{5r^3} + \frac{r_0^4\rho_2(r_0)}{4r^2} \tag{A8}$$

Evidently, the potential is of the desired form for $r > r_0$ provided that $\rho_2(r)$ for $r < r_0$ obeys the simple integral constraint that $K = 0$. Only for $r > r_0$ is the potential of separable form. Orbits whose pericenters satisfy $r_\mathrm{p} > r_0$ lie within rectangular toroids and have three exact integrals of motion.

APPENDIX B: ALIGNMENT IN ELLIPSOIDAL COORDINATES

Ellipsoidal coordinates (λ,μ,ν) are the most natural coordinates to study triaxial stellar systems (e.g., Lynden-Bell 1962; de Zeeuw 1985; van de Ven et al. 2003; Sanders & Evans 2015). The scale factors are

$$\begin{aligned} P^2 &= \frac{(\lambda-\mu)(\lambda-\nu)}{4(\lambda+a)(\lambda+b)(\lambda+c)},\\ Q^2 &= \frac{(\mu-\lambda)(\mu-\nu)}{4(\mu+a)(\mu+b)(\mu+c)},\\ R^2 &= \frac{(\nu-\mu)(\nu-\lambda)}{4(\nu+a)(\nu+b)(\nu+c)}, \end{aligned} \tag{B1}$$

where a, b and c are constants that define two sets of foci. Surfaces of constant λ, μ and ν are confocal ellipsoids, one-sheeted hyperboloids and two-sheeted hyperboloids respectively. The coordinate system is illustrated in e.g., Hilbert & Cohn-Vossen (1999), de Zeeuw (1985) or Boccaletti & Pucacco (1996).

We start by assuming that the velocity ellipsoid is diagonalised in confocal ellipsoidal coordinates, so that all the cross-terms $\langle v_\lambda v_\mu\rangle$, $\langle v_\lambda v_\mu\rangle$ and $\langle v_\mu v_\nu\rangle$ all vanish. The Hamiltonian is:

$$H = \frac{1}{2}\Big(\frac{p_\lambda^2}{P^2} + \frac{p_\mu^2}{Q^2} + \frac{p_\nu^2}{R^2}\Big) - \psi(\lambda,\mu,\nu), \tag{B2}$$

where $p_\lambda = P^2\dot\lambda$, $p_\mu = P^2\dot\mu$ and $p_\nu = P^2\dot\nu$ are canonical momenta. Again, as the Hamiltonian is time-invariant, we can always construct the even part of the DF as depending on the squares of the canonical momenta only. For the cross-terms to vanish in ellipsoidal coordinates, this means $F_\mathrm{e} = F_\mathrm{e}(p_\lambda^2, p_\mu^2, p_\nu^2, \lambda,\mu,\nu)$. Using the Hamiltonian to eliminate p_λ^2 without loss of generality, we obtain $F_\mathrm{e}(H, p_\mu^2, p_\nu^2, \lambda,\mu,\nu)$. Taking the Poisson bracket $\{F_\mathrm{e}, H\} = 0$ tells us that F_e is independent of λ as well as p_λ. We find, after some work,:

$$A_1\frac{\partial F_\mathrm{e}}{\partial p_\mu} + A_2\frac{\partial F_\mathrm{e}}{\partial p_\nu} = \frac{p_\mu}{Q^2}\frac{\partial F_\mathrm{e}}{\partial\mu} + \frac{p_\nu}{R^2}\frac{\partial F_\mathrm{e}}{\partial\nu} \tag{B3}$$

with

$$A_1 = \frac{1}{\lambda-\mu}\left[\frac{p_\mu^2}{2}\frac{\partial}{\partial\mu}\left(\frac{\lambda-\mu}{Q^2}\right) + \frac{p_\nu^2}{2}\frac{\partial}{\partial\mu}\left(\frac{\lambda-\mu}{R^2}\right) - \frac{\partial}{\partial\mu}\left((\lambda-\mu)\psi\right) + H\right] \tag{B4}$$

and

$$A_2 = \frac{1}{\lambda-\nu}\left[\frac{p_\mu^2}{2}\frac{\partial}{\partial\nu}\left(\frac{\lambda-\nu}{Q^2}\right) + \frac{p_\nu^2}{2}\frac{\partial}{\partial\nu}\left(\frac{\lambda-\nu}{R^2}\right) - \frac{\partial}{\partial\nu}\left((\lambda-\nu)\psi\right) + H\right] \tag{B5}$$

We are at liberty to send $p_\mu \to -p_\mu$ or to send $p_\nu \to -p_\nu$ as the DF is invariant under such changes. This tell us that the two equations

$$\begin{aligned} A_1\frac{\partial F_\mathrm{e}}{\partial p_\mu} &= \frac{p_\mu}{Q^2}\frac{\partial F_\mathrm{e}}{\partial\mu},\\ A_2\frac{\partial F_\mathrm{e}}{\partial p_\nu} &= \frac{p_\nu}{R^2}\frac{\partial F_\mathrm{e}}{\partial\nu}, \end{aligned} \tag{B6}$$

must be separately satisfied. Now, take the first equation, multiply by $(\lambda-\mu)$ and differentiate with respect to λ. We already know that F_e is independent of λ and that H may be treated as a constant, so this operator annihilates all terms bar the one containing the potential and leaves us with

$$\frac{\partial^2}{\partial\lambda\partial\mu}\Big((\lambda-\mu)\psi\Big) = 0. \tag{B7}$$

Similarly, multiplying the second equation by $(\lambda-\nu)$ and differen-

tiating with respect to λ leaves us with

$$\frac{\partial^2}{\partial\lambda\partial\nu}\Big((\lambda-\nu)\psi\Big)=0. \tag{B8}$$

We could of course have started by eliminating p_μ^2 in terms of the Hamiltonian, and repeating our steps would yield

$$\frac{\partial^2}{\partial\mu\partial\nu}\Big((\mu-\nu)\psi\Big)=0. \tag{B9}$$

This gives us three partial differential equations that the potential must satisfy, and it is straightforward to integrate them up to establish

$$\psi(\lambda,\mu,\nu)=\frac{f_1(\lambda)}{(\lambda-\mu)(\lambda-\nu)}+\frac{f_2(\mu)}{(\mu-\lambda)(\mu-\nu)}+\frac{f_3(\nu)}{(\nu-\lambda)(\nu-\mu)} \tag{B10}$$

where $f_1(\lambda)$, $f_2(\mu)$ and $f_3(\nu)$ are arbitrary functions of the indicated arguments. This is the separable or Stäckel potential in confocal ellipsoidal coordinates.

APPENDIX C: THE STÄCKEL CONDITION

Rather than demonstrating the theorem for each alignment separately, a more mathematical – but abstract – approach is to derive all possible coordinate systems and gravitational potentials together. This is similar in spirit to the original investigations of Stäckel (1891) and Eddington (1915).

Here, we prove the following theorem. *Suppose that (i) the velocity dispersion tensor of a stellar system is aligned in an orthogonal curvilinear coordinate system and has (in general) three unequal axes and that (ii) the stellar system is in a steady state, so that the even part of the distribution function (DF) must satisfy the collisionless Boltzmann equation. Then, it necessarily follows that the coordinate system is the confocal ellipsoidal coordinates (or one of its limiting cases) and that the gravitational potential is of separable or Stäckel form.*

Consider a system with 3 degrees of freedom governed by the Hamiltonian of the form of

$$H=\frac{1}{2}\sum_k\frac{p_k^2}{\mathsf{h}_k^2(q_1,q_2,q_3)}-\psi(q_1,q_2,q_3), \tag{C1}$$

where (q_1,q_2,q_3) are orthogonal curvilinear coordinates, (p_1,p_2,p_3) are the corresponding canonical momenta and h_1,h_2,h_3 are the scale factors. Suppose that the system admits an integral of motion of the form, $F_{\rm e}=F_{\rm e}(p_1^2,p_2^2,p_3^2;q_1,q_2,q_3)$ which is recognised as the even part of the DF. The vanishing of the Poisson bracket requires

$$\begin{aligned}\dot{F}_{\rm e} &= \{F_{\rm e},H\}=\sum_i\left(\frac{\partial F_{\rm e}}{\partial q_i}\frac{\partial H}{\partial p_i}-\frac{\partial H}{\partial q_i}\frac{\partial F_{\rm e}}{\partial p_i}\right)\\ &= \sum_i p_i\left(\frac{1}{\mathsf{h}_i^2}\frac{\partial F_{\rm e}}{\partial q_i}-2\frac{\partial H}{\partial q_i}\frac{\partial F_{\rm e}}{\partial(p_i^2)}\right)=0.\end{aligned} \tag{C2}$$

However, both H and $F_{\rm e}$ are invariant under $p_j\to-p_j$ for any j's, and so it follows that, for $\forall i\in\{1,2,3\}$,

$$\frac{\partial F_{\rm e}}{\partial q_i}=\zeta_i\frac{\partial H}{\partial q_i},\quad \zeta_i\equiv 2\mathsf{h}_i^2\frac{\partial F_{\rm e}}{\partial(p_i^2)}. \tag{C3}$$

Here note that, for any i and j,

$$\begin{aligned}\frac{\partial\zeta_i}{\partial q_j} &= 2\mathsf{h}_i^2\frac{\partial^2F_{\rm e}}{\partial q_j\partial(p_i^2)}+2\frac{\partial\mathsf{h}_i^2}{\partial q_j}\frac{\partial F_{\rm e}}{\partial(p_i^2)}\\ &= 2\mathsf{h}_i^2\frac{\partial}{\partial(p_i^2)}\left(\zeta_j\frac{\partial H}{\partial q_j}\right)+\frac{\zeta_i}{\mathsf{h}_i^2}\frac{\partial\mathsf{h}_i^2}{\partial q_j}\\ &= 2\mathsf{h}_i^2\frac{\partial\zeta_j}{\partial(p_i^2)}\frac{\partial H}{\partial q_j}+2\mathsf{h}_i^2\zeta_j\frac{\partial^2H}{\partial(p_i^2)\partial q_j}+\frac{\zeta_i}{\mathsf{h}_i^2}\frac{\partial\mathsf{h}_i^2}{\partial q_j}\\ &= 4\mathsf{h}_i^2\mathsf{h}_j^2\frac{\partial^2F_{\rm e}}{\partial(p_i^2)\partial(p_j^2)}\frac{\partial H}{\partial q_j}+\mathsf{h}_i^2\zeta_j\frac{\partial}{\partial q_j}\left(\frac{1}{\mathsf{h}_i^2}\right)+\frac{\zeta_i}{\mathsf{h}_i^2}\frac{\partial\mathsf{h}_i^2}{\partial q_j}\\ &= 4\mathsf{h}_i^2\mathsf{h}_j^2\frac{\partial^2F_{\rm e}}{\partial(p_i^2)\partial(p_j^2)}\frac{\partial H}{\partial q_j}+\frac{\zeta_i-\zeta_j}{\mathsf{h}_i^2}\frac{\partial\mathsf{h}_i^2}{\partial q_j}\end{aligned} \tag{C4}$$

Then the integrability condition on $F_{\rm e}$ is

$$\frac{\partial}{\partial q_i}\left(\frac{\partial F_{\rm e}}{\partial q_j}\right)-\frac{\partial}{\partial q_j}\left(\frac{\partial F_{\rm e}}{\partial q_i}\right)=0 \tag{C5}$$

which results in

$$\begin{aligned}&\frac{\partial}{\partial q_i}\left(\zeta_j\frac{\partial H}{\partial q_j}\right)-\frac{\partial}{\partial q_j}\left(\zeta_i\frac{\partial H}{\partial q_i}\right)\\ =\;&\frac{\partial\zeta_j}{\partial q_i}\frac{\partial H}{\partial q_j}-\frac{\partial\zeta_i}{\partial q_j}\frac{\partial H}{\partial q_i}+\zeta_j\frac{\partial^2H}{\partial q_i\partial q_j}-\zeta_i\frac{\partial^2H}{\partial q_j\partial q_i}\\ =\;&\frac{\zeta_j-\zeta_i}{\mathsf{h}_j^2}\frac{\partial\mathsf{h}_j^2}{\partial q_i}\frac{\partial H}{\partial q_j}-\frac{\zeta_i-\zeta_j}{\mathsf{h}_i^2}\frac{\partial\mathsf{h}_i^2}{\partial q_j}\frac{\partial H}{\partial q_i}+(\zeta_j-\zeta_i)\frac{\partial^2H}{\partial q_i\partial q_j}\\ =\;&(\zeta_j-\zeta_i)\,\mathcal{D}_{ij}(H)=0\quad\text{(for all } i,j).\end{aligned} \tag{C6}$$

Here, $\mathcal{D}_{ij}(f)$ is the linear second-order differential operator acting on a function $f(q_1,q_2,q_2)$, defined as

$$\begin{aligned}\mathcal{D}_{ij}(f) &\equiv \frac{1}{\mathsf{h}_j^2}\frac{\partial\mathsf{h}_j^2}{\partial q_i}\frac{\partial f}{\partial q_j}+\frac{1}{\mathsf{h}_i^2}\frac{\partial\mathsf{h}_i^2}{\partial q_j}\frac{\partial f}{\partial q_i}+\frac{\partial^2f}{\partial q_i\partial q_j}\\ &= \left(\frac{\partial\ln\mathsf{h}_j^2}{\partial q_i}\frac{\partial}{\partial q_j}+\frac{\partial\ln\mathsf{h}_i^2}{\partial q_j}\frac{\partial}{\partial q_i}+\frac{\partial^2}{\partial q_i\partial q_j}\right)f,\end{aligned} \tag{C7}$$

which is symmetric for $i\leftrightarrow j$, i.e. $\mathcal{D}_{ij}(f)=\mathcal{D}_{ji}(f)$. In other words, if there exists an integral $F_{\rm e}$, we must have $\zeta_i=\zeta_j$ or $\mathcal{D}_{ij}(H)=0$ for any pair of indices i and j. The $\zeta_i=\zeta_j$ (for $i\neq j$) case however implies that the integral $F_{\rm e}$ becomes invariant under the rotation within p_i-p_j plane and so the distribution must be isotropic within q_i-q_j plane: that is to say, the resulting velocity dispersion must be degenerate as in $\langle v_i^2\rangle=\langle v_j^2\rangle$. If $\zeta_i\neq\zeta_j$ on the other hand, we must have

$$\mathcal{D}_{ij}(H)=\frac{1}{2}\sum_k\mathcal{D}_{ij}\left(\frac{1}{\mathsf{h}_k^2}\right)p_k^2-\mathcal{D}_{ij}(\psi)=0\quad\Rightarrow\;\mathcal{D}_{ij}(\mathsf{h}_k^{-2})=\mathcal{D}_{ij}(\psi)=0 \tag{C8}$$

The condition on the scale factors $\mathcal{D}_{ij}(\mathsf{h}_k^{-2})=0$ for all $i\neq j$ (and any k) is the same condition defining the Stäckel systems. The most general orthogonal curvilinear coordinate in a Euclidean space that satisfies the condition is the confocal ellipsoidal coordinates. This encompasses the 11 3-D quadric coordinates in which the Helmholtz equation separates (Morse & Feshbach 1953). On the other hand, the general solution of $\mathcal{D}_{ij}(\psi)=0$ in the confocal ellipsoidal coordinates (or its degenerate limit) is known to be $\psi(q_1,q_2,q_3)=\sum_k f_k(q_k)/\mathsf{h}_k^2$ where $f_k(q_k)$ is an arbitrary function of the coordinate component q_k alone.

The condition $\mathcal{D}_{ij}(\psi)=0$ is really the integrability condition on the system of the quasi-linear partial differential equations. If we suppose the existence of the set of functions $\{f_k(q_k)\}$ such that

$\psi(q_1, q_2, q_3) = \sum_k f_k(q_k)/\mathsf{h}_k^2$, then

$$\frac{\partial\psi}{\partial q_i} = \frac{f_i'(q_i)}{\mathsf{h}_i^2} - \sum_k \frac{\partial \mathsf{h}_k^{-2}}{\partial q_i} f_k(q_k) \quad \Rightarrow \quad \frac{\partial f_i}{\partial q_j} = \delta_i^j \mathsf{h}_i^2 \left(\frac{\partial\psi}{\partial q_i} + \sum_k \frac{\partial \mathsf{h}_k^{-2}}{\partial q_i} f_k \right).$$

where δ_i^j is the Kronecker delta. This is the system of partial differential equations on $\{f_k(q_1, q_2, q_3)\}$, whose compatibility condition implies that $(\partial/\partial q_j)(\partial f_i/\partial q_k) = (\partial/\partial q_k)(\partial f_i/\partial q_j)$ for any i, j, k. The only non-trivial conditions among these are

$$\frac{\partial}{\partial q_j}\left(\frac{\partial f_i}{\partial q_i}\right) = \mathsf{h}_i^2 \left[\mathcal{D}_{ij}(\psi) - \sum_k \mathcal{D}_{ij}(\mathsf{h}_k^{-2}) f_k \right] = 0 \quad \text{(for any } i \neq j\text{)},$$

and so, given the Stäckel coordinate satisfying $\mathcal{D}_{ij}(\mathsf{h}_k^{-2}) = 0$, we find that $\mathcal{D}_{ij}(\psi) = 0$ is the necessary condition for existence of the solution set $\{f_k\}$. Moreover, thanks to the Frobenius theorem, the condition is also sufficient for (local) existence of such a solution set. In other words, $\psi(q_1, \ldots, q_n) = \sum_k f_k(q_k)/\mathsf{h}_k^2$ is also in fact the general solution of $\mathcal{D}_{ij}(\psi) = 0$.

Finally, we remark that the results in this appendix are readily generalised to N degrees of freedom.